A Bioimpedance System for Fluid Monitoring in Dengue Disease

Master's Thesis

Abhilash Guru Dutt
M.Sc Biomedical Engineering
TU-Delft

June 7, 2020

Project Supervisor:	Prof. Dr. Walter Karlen Mobile Health Systems Laboratory, ETH Zurich
Internal Supervisor:	Prof. Dr. P J French Bioelectronics, TU - Delft
Thesis Committee:	Dr. T. Costa (Bioelectronics, TU Delft) Dr. V. Giagka (Bioelectronics, TU Delft) Dr. Ir. Alfred C. Schouten (3mE, TU Delft)

Abstract

Dengue disease is a mosquito borne viral fever widespread in tropical and subtropical regions of the world. The incidence of the disease has rapidly grown over the last decade. There is no specific course of medication to treat dengue. But determining the intensity of fluid leakage is essential in managing the progression of the disease. Bioimpedance technology is an inviting tool for safe, inexpensive and non-invasive monitoring of body fluids. However existing systems are not attractive for continuous and long term assessments. In addition the system performance is also susceptible to variations in posture and motion related artifacts. This work presents a motion aware bioimpedance measurement system (AMBICA) for fluid monitoring using AD5940 and accelerometers to overcome the mentioned limitations. The primary aim of this thesis is to characterize the performance of the developed device with a commercial device(BIACorpus). Additionally a framework to detect the variation in posture and motion is presented.Bioimpedance and movement data was collected from 14 healthy volunteers. The impedance values measured by the device showed high correlation ($r>0.98$) while the reactance values showed weak correlation ($0.10 < r < 0.67$). The bias and limits of agreement estimated for impedance measurements are $-4.50\pm13.01\Omega$ and $[21.0,-30.0]\Omega$ respectively. The estimated bias and limits of agreement for reactance measurements are $14.84\pm19.64\Omega$, the limits of agreement are $[53.36,-23.68]\Omega$. The precision scores indicated a higher variability in measurements for BIACorpus device compared to AMBICA. The proposed framework was able to identify the active and inactive periods and gross postures like supine, sitting and standing with an accuracy of $>95\%$ and 94.6% respectively. The results in this study showed that the impedance and reactance values followed a typical trend agreeable with bioimpedance measurements. However, the values measured by AMBICA agree more closely with BIACorpus for impedance measurements than for reactance measurements. Inconsistencies are observed for both devices and they are attributed to parasitics and imbalance of interface impedances at the inputs of the AD5940. Due to the difference in technologies used, the values from the devices do not measure the exact same values. Therefore values above or below the reference values may still have clinical significance. AMBICA can be used in the future for fluid assessments in dengue affected subjects. Furthermore motion related information gathered using the framework proposed can be further incorporated to develop contextual bioimpedance monitoring applications.

Acknowledgements

I would like to express my gratitude to my research supervisor Professor Dr. Walter Karlen for firstly giving me an opportunity to conduct my thesis at the Mobile Health Systems Lab. He gave me the freedom to be creative with my research and motivated and supported me throughout my project. I am particularly grateful for all that I have learnt from Walter through our wealthy discussions related to the important aspects of biomedical systems,PCB design and CAD models.

I would like to thank the entire team of the Mobile Health Systems Lab for all the support, motivation and kind friendship ,making my stay at the lab a comfortable and a memorable one. Working at the lab has been a very rewarding experience.

I would like to thank the Dr Louise Thwaithes, Dr Hoang Minh Tu Van, Khanh Phan and the entire team of the Emerging Infections Group at the Oxford University Clinical Research Unit - Vietnam for having Michaela and myself over at the research facility in Vietnam, assisting the team with the clinical experiments and also for providing an opportunity to visit the Intensive Care Units to learn about the specific requirements for the bioimpedance system.

I would like to extend my thanks to Michaela Verling who made the clinical study in this thesis possible and for being such a valuable and fun colleague who made the travel to OUCRU a memorable one.

I would like to thank my TU-Delft supervisor Professor Dr. Paddy French. He was extremely supportive throughout the research project and provided valuable feedback regarding the same. Moreover, I enjoyed the highly educational conversations I shared with him during the Sensors & Actuators and Systems Engineering course.

I would also like to thank the members of the Exercise Physiology Lab who were kind to lend the BIACorpus bioimpedance measurement system for this thesis.

Finally,I would like to thank my family and friends who have supported and encouraged me during my entire time as a master student.

Contents

List of Figures

List of Tables

Chapter 1

Introduction

Dengue is a mosquito borne viral fever caused by dengue virus. The disease is mostly prevalent in tropical and sub-tropical regions of the world. The disease is a global burden and a recent estimate by the World Health Organization reports nearly 390 million cases of dengue infections over which 96 million manifest clinically [1]. Typically the fever manifests itself in four stages viz incubation period, febrile illness, critical phase and recovery phase.

Clinical researchers have associated the onset and initial stages of the infection with an increase in plasma volume and severe hypertensive shocks that will eventually cause the circulatory system to fail. If this stage is not treated and more importantly not managed well by the clinician, the progression towards the fatal stages is rapid and painful.

Unfortunately, there is no specific treatment available for dengue hemorrhagic fever apart from preventive and supportive care like fluid replacement therapy and platelet transfusion which is extremely critical in order to control the progression of the disease [2].

Currently, the two techniques used to characterize the disease prognosis are, observing the progression of plasma leakage and monitoring the platelet counts. With the latter every time the platelet drops below 20,000 cell/mm^2,the patient is subjected to platelet transfusions. The use of platelet transfusion technique increases the chance of febrile non hemolytic reaction, allergies and bacterial sepsis. In addition this strategy takes a long time and requires periodical blood sampling for laboratory analysis and therefore it is not a very attractive solution. Tracking plasma leakage requires repeated assessment for pleural effusion and ascities either through blood draws, imaging and hematocrit assessment. While the former is invasive the latter is not convenient for repeated assessments keeping in mind exposure to radiation and cost.

Researchers have consequently looked for alternative predictive techniques to successfully identify the condition of dengue to improve the triage. Recently bio-electrical impedance analysis approach was incorporated to classify the risks in dengue fever [3]. The principal motivation for using bio-electrical impedance for dengue shock classification is the ability of the technique to estimate the plasma leakage through fluid status monitoring. Investigations regarding the approach have shown promising and notable outcomes and has opened up a lot of opportunities.

Theoretically, bio-impedance measurements allow the estimation of fluid levels in the body compartments by utilizing the property of differential response of the body towards high and low frequency alternating current. Several techniques have rolled out since, to model and determine fluid levels like single frequency bio-impedance analysis(BIA), multi frequency BIA and bio-impedance spectroscopy. However, the existing commercial measurement systems are bulky, expensive and not suited for continuous and long term fluid status monitoring. In the clinical setting the bio-impedance devices needs to be deployed in care units where the movement of the person is restricted beyond activities of daily living. But the bioimpedance signal is extremely sensitive to postural variations and movement artifacts. The commercial systems do not account for these adverse physio-environmental parameters. In addition the systems require strict conformance to measurement protocols in clinical settings.

With the recent advancements in bio-signal sensing technology, these limitations can be addressed. The reduced size and increased computational power of electronic components have provided keen opportunities to develop devices with 'awareness'. A device such as this would not only be able to measure bio-impedance continuously for a long time , but would also be able to perform several intelligent tasks to sense the surroundings and create clinical contexts to support decision making.

Therefore the bio-impedance system put forth in this work envisions to bridge the gap between clinical challenges and technical solutions to tailor a device that can be used in the clinical setting.

1.1 Focus of this Work

To that extent, this work primarily focuses on developing a prototype version of a bio-impedance measurement system that is comparable in performance to an existing commercial device. Additionally a framework is proposed that would allow the measurement system to be motion aware with the capability to obtain movement and position specific information.

The main contributions of this work are

- Comparing the performance of the developed bio-impedance monitoring system with a commercially established system to characterize the performance and validity of the newly developed system.
- A prototype system that incorporates an analog front end for bio-impedance monitoring and digital accelerometers that allow the system to monitor bio-impedance while having the capability to be motion aware.

1.2 Thesis Organization

The thesis is organized into the following sections

- Chapter 2 : Introduces bioimpedance and bioimpedance techniques.The design considerations for a bioimpedance measurement system along with a focused review on the performance comparison of the previously developed devices.
- Chapter 3 : Describes in detail the development of the bioimpedance system and the experimental study.The chapter also provides information regarding analytical approaches utilized in this work.
- Chapter 4 : This chapter presents the results and discussions from the findings of this this work. The first section presents the participant demographics data. The second and third section describes and discusses the findings to compare the developed device against the reference device. The last section describes and discusses the findings from the framework proposed for gathering movement related information for contextual monitoring.
- Chapter 5 : Concludes the thesis with an overview of the important finding of this work.

Chapter 2

Background

Non-invasive fluid management is vital for monitoring clinical conditions such as dengue. The critical parameter to estimate is the percentage changes of fluid and hydration levels of the patient. Traditionally, isotope dilution and total body potassium have been used for fluid monitoring [4]. But these techniques are invasive, expensive and inaccurate for detecting small changes in fluid levels and are not suited for point of care long term monitoring. On contrary, bio-impedance analysis allows non-invasive, safe and inexpensive long term point of care fluid assessments. Bio-impedance in a generic sense is the impedance offered by the human body as a response to an applied alternating electrical current due to underlying tissue level electro-chemical reaction.

The following section describes the bio-electrical basis of the signal and the principal behind using bio-impedance to assess fluid levels in the body.

2.1 Bio-Electrical Basis of Bio-Impedance

The electrical behavior in the human body is largely dependent on various bio-chemical phenomena in the cells and tissues. The ions dissolved within the body aids in electrical conduction. Therefore the electrolytic theory is fundamental to explain conductivity within the human body. The electrolytic theory highlights that the amount of charges that can flow in cells and tissues is directly proportional to the concentration of dissolved ions [5]. The electrical resistance of cells and tissues increases or decreases if the concentration of the dissolved ions decreases or increases respectively. Apart from this, the electrical impedance of cells and tissues is also dependent on the permittivity of dielectric substances in the body. Therefore the analysis of bio-impedance involves the interplay between conductivity and permittivity.

Structural characterization of human cells have provided deeper insights regarding the origins of bio-impedance and its relation with conductivity and permittivity. The cells in our body are composed of intra-cellular fluids (ICF) enveloped inside a cell membrane (CM) and suspended in a extra-cellular fluidic (ECF) matrix as shown in Figure 2.1. The ICF is primarily composed of solutions of protein,salts and water.

The ECF is also an electrolyte rich solution comprised of ionic solutions of highly conducting salts and thus from the above theory it is comprehensible that ICF and ECF are conductive and offer low resisting paths to an applied electrical signal [6].

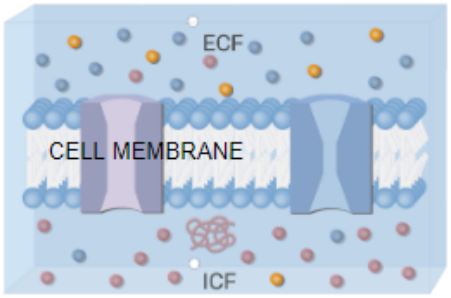

Figure 2.1: Cross sectional view of a typical cell[7]

The cell membrane however, exhibits a different behavior due to its complex structure. The cross section of the membrane is a protein-lipid-protein sandwiched structure and manifests itself as a dielectric membrane between two conducting fluid medium. This resembles the behavior of a capacitor.

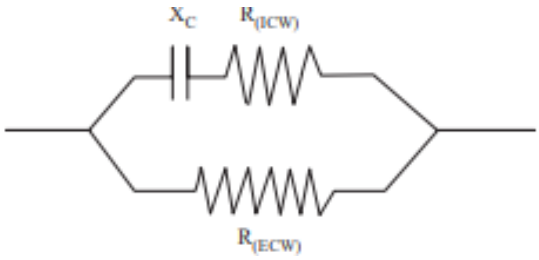

Figure 2.2: 2R-C Model of a Cell [8]

Altogether, the human cells offers a complex valued bio impedance quantity (Z) to an applied alternating electrical signal wherein ECF and ICF contributes to the resistive quantity (behaves as resistors) and CM contributes to the reactive quantity (behaves as a capacitor). The equivalent 2R-C electrical model is shown in Figure 2.2. In this model R_e(R_ECF) and R_i(R_ICF) represents the resistance offered by the ECF and ICF respectively. The CM is modeled as the capacitor.While the 2R-C model is the ideal model, a more descriptive model used to explain the bio-impedance signals is the cole model. The cole model assumes the CM as a constant phase element whose behavior depends on α. When α is equal to 0 the CM behaves as a resistor and when it equals to 1 the CM behaves as a capacitor.

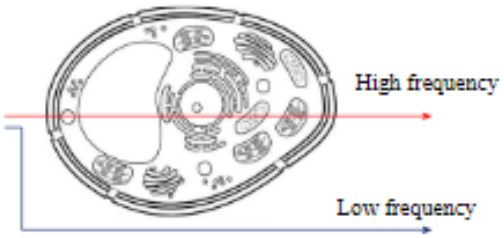

Figure 2.3: Flow of current at low and high frequency

Tissues as a network of resistors and capacitors have an important role in the conduction of the applied alternating electrical signal within the body. Low frequency electrical signals travel around the cells and through the ECF as the capacitor offers a higher impedance at lower frequencies. Conversely, higher frequency electrical signals penetrates through the cells as the capacitor offers a lower impedance. The equivalent impedance at high frequency is Re||Ri as the capacitor can be assumed as a short circuit. The flow of electrical signal at different frequencies is illustrated in Figure 2.3. This differential behavior helps in estimating the extra cellular and intra cellular fluid volumes.

2.2 Estimation of Fluid Volume and Hydration Status

The previous section described the origin of the bio-impedance signal. It was also mentioned that the impedance offered to the flow of alternating current is a vector which has a real quantity (the resistance as offered by the intra and extra cellular fluids) and imaginary quantity (the capacitive impedance offered by the cellular membrane).

To interpret bio-impedance measurements into fluid volume estimates like total body water and extracellular water, it is convenient to view the body as a cylindrical volume conductor with intrinsic properties such as resistivity & conductivity and geometric parameters like cross sectional area and length [9].

With the prior knowledge of the model (body as multiple cylindrical conducting compartments) and the measured bio-impedance, it is possible to estimate the fluid volume by two main principles namely bioimpedance analysis and bioimpedance spectroscopy.

2.2.1 Bio Impedance Analysis

This analysis technique estimates the total body water (TBW), intra cellular water (ICW) and extra cellular water (ECW) using whole body bio-impedance measurements as shown in Figure 2.4 or segmental bio-impedance measurements performed using a single frequency (SF-BIA) or multiple frequencies (MF-BIA). SF-BIA is performed at 50kHz while MF-BIA is performed over a range of frequencies from 1kHz to 500kHz.

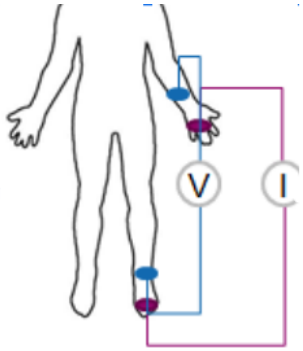

Figure 2.4: 4 wire BIA set-up

Considering the body as a cylindrical conductor with constant resistivity and geometric variables, the resistance of the cylinder can be determined by Equation 2.1. L is the length of the volume conductor, A is the cross sectional area and ρ is the resistivity of the conductor [10].

$$R = \rho * \frac{L}{A} \tag{2.1}$$

Equation in 2.1 can be re-arranged to estimate the volume of fluid. Considering that the measured bio-impedance is R and the cylindrical volume conductor has similar intrinsic properties as described earlier, the volume can be estimated by using the Equation 2.2.

$$Volume = \rho * \frac{L^2}{R} \tag{2.2}$$

Volume estimates based on this principle is dependent on frequency. As discussed in the previous section. Low frequency signals prefer to travel through the ECF. Thus at low frequency impedance measurements only the ECW is estimated. Conversely, at high frequencies the electrical current passes completely through the cell and therefore reflects the TBW. The difference between the two estimated volume quantities determine the value of ICW. However this techniques has a couple of drawbacks.

Firstly, the technique uses regression analysis to model equations that estimate volume based on the measured $\frac{L^2}{R}$ values and anthropometric factors such as age and weight. Secondly, it assumes the human body as a homogeneous cylindrical volume conductor with constant resistivity through out the length of the conductor which is an ideal assumption.

2.2.2 Bio-Impedance Spectroscopy(BIS)

BIS categorizes the body into three cylindrical conductive compartments namely the arm, leg and trunk. BIS measures the impedance over the frequency range of 1kHz to 1MHz. The fluid volume estimates are then determined by mathematically predicting the resistances at zero frequency and infinite frequency with curve-fitting on a reactance vs resistance curve [11]. BIS also considers the behavior of the tissues at intermediate frequencies. At these frequencies the impedance measured is between resistance at infinite frequency and resistance at zero frequency and is dependent on the phase difference. A typical Xc vs R graph used for BIS is illustrated in Figure 2.5. The illustration shows the progression from zero frequency to infinite frequency. The peak of the curve represents the resonance characteristic frequency fc. The value of fc is determined by the parameters of the earlier circuit model and the equation shown in Equation 2.3.

Fluid volume estimation by BIS involves initially estimating the resistances at infinite frequency and zero frequency by the cole plot and mathematical curve fitting. Subsequently, the extracellular body volume is estimated by BIS techniques using Equation 2.4. The parameter k is a constant derived based on anthropometric values and W is the body weight. Calculation of TBW is performed similarly with the resistance R replaced by resistance at infinite frequency.

$$fc = \frac{1}{2 * pi * Cm * (Re + Ri)} \tag{2.3}$$

$$ECW = k * (\frac{L^2 * W^{\frac{1}{2}}}{R})^{\frac{2}{3}} \tag{2.4}$$

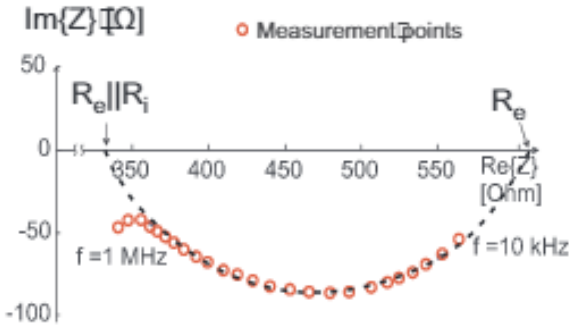

Figure 2.5: Illustration of BIS Xc vs R plot .Source : Ulbrich et al[12]

BIS has it's own limitations. The resistivity of the three cylinders are approximated, parameter k is approximated and the validity is based on accurate curve fitting to derive the resistance at extreme frequencies.

2.2.3 Hydration Status

A popular method considered to determine hydration status is through the estimation of $\frac{ECW}{TBW}$. BIS technique is used to measure the ECW and TBW as mentioned previously and the ratio is computed. A normal hydration threshold is defined clinically based on multiple measurements with the device. A ratio above this threshold indicates over hydration and below the threshold indicates de-hydration.

2.3 Bio-Impedance Measurement System Design Considerations

In order to facilitate bio-impedance measurements various systems have been developed in the past. The unerring measurement of bio-impedance is influenced by the physiological factors, interfaces between the device and the human tissue and technical sub-systems. This section only describes certain important criteria that influence the design considerations for a bio-impedance measurement system.

2.3.1 Electrode-Electrolyte-Skin Interface & Motion Artifacts

As mentioned previously, bio-impedance is the response of the human tissue to alternating electrical signal. To couple the unit that injects the signal with the human tissue and to re-couple the human tissue back to signal measurement unit an electrode is used. The introduction of electrodes onto the surface of the human body creates two vital interfaces.

The electrode-electrolyte interface and the electrolyte-skin interface. Even when no signal is introduced through the electrodes, an electrical double layers is formed through local distribution and arrangement of charges across the interface. The charges across the interface induce an homeostatic potential difference between the conducting medium (electrolyte) and the conductor.On the other hand, when a signal is introduced through the electrode, there is a mutual exchange of charge carriers between the conducting medium and electrode through redox reactions and charge re-distribution across the double layer. Revisiting the electro-chemical theory, the latter is said to be non faradaic and a representation of the capacitance of the charged double layer. The former is therefore a faradaic process that involves redox reactions in an electrolytic medium [13]. As a result the interface between the electrode and electrolyte can be modeled as a network of resistors and capacitors. A representation of this model is shown in Figure 2.6. The voltage source 'V_H' represents the half-cell potential arising due to the initial redistribution of charges when no external signal is introduced.

Artifacts are generated as consequence of the change in the electrical properties at the interface. In an ideal condition, when a signal passes across the tissue there is pure conduction (through redox reactions) through the interfaces without any potential drops along the conducting medium.

However, in the case of motion artifacts, movement induces a relative shift of the electrodes at the interface, resulting in the redistribution of charges at the interface which appears as a potential at the input of the measuring system. The potential generated is highly variable and dependent on the relative orientation at the interfaces. The greyed segment in the Figure 2.6 corresponds to the changing conditions at the interface due to relative motion [14]. The additive artifact potential interferes with the bio-impedance signal and reduces the quality of measured signal.

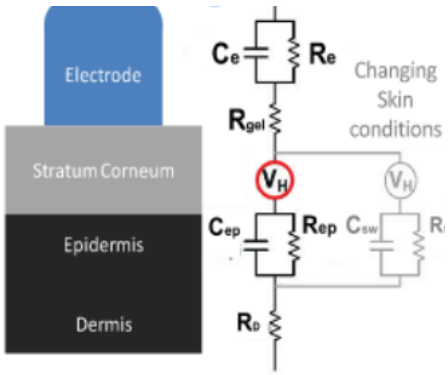

Figure 2.6: Skin-Electrode interface Illustration [14]

The cause of motion artifact generation can be due to the gross movement of the part with the electrode on it or even micro movements such has skin stretching which can induce a spiky artifact potential of about 5mV[15]. Artifacts therefore do not enable the measurement system to faithfully reproduce the bio-impedance signal and reduces the clinical utility of the signals.

Mitigation of artifacts at the source is rather quite challenging. Unconventional approaches such has soft padded and hard padded supports [16] have been used to remove the effect at the source. However this solution is not very effective and requires additional contraptions that the individual might find uncomfortable and possibly even cause biocompatibility issues. Electrode system configuration as discussed in subsection 2.3.4 can be employed to make certain intermediate impedances at the interface redundant. But to be able to completely remove the effects of artifacts either very sophisticated hardware solutions like transient gain adjustments and heterodyning with a frequency feedback [17] or online digital signal processing techniques can be employed. The former techniques although extravagant and effective require extremely precise analog instrumentation that requires additional signal converters. This increases the overall development costs. In addition the technique requires efficient power management. With the development of low power, high computational components, it is a lot convenient to tackle this issue online using signal processing. To that extent literature suggests various approaches from various adaptive filtering techniques [18], bayesian filtering approaches such as kalman filters and particle filters, wavelet analysis and independent component analysis [19]. Without discussing the individual solutions in detail, the favoured approach to remove movement related artifacts with efficient system power consumption and computation is by utilizing an additional sensor that has the ability to generate motion reference frame to detect the changing surroundings. The claim has been sustained with the development of low cost precise inertial measurement units. Overall, the susceptibility of bio-impedance signal to motion artifacts has been deeply emphasised and therefore requires the development of solutions to negate its influence on the measurement system.

2.3.2 Postural Effects on Bio-impedance

Hydro-static pressure and force of gravity have an impact on fluid distribution in our body. When an individual changes his position, there is a slight change in the blood pressure as a consequence of the former two forces. An illustration of the difference in pressures during different positions is shown in Figure2.7. In addition to the variation in blood pressure there is rapid regulation of blood and plasma volumes in the interstitial spaces [20]. Fluids tend to shift from the plasma space and the interstitial space. For instance, when a person is in a supine position, the fluids move into the plasma space and the plasma volume increases. Therefore transient changes in human posture affects the distribution of fluids in various compartments of the body.

Re-distribution of fluid volumes due to position variations in the human body changes the intrinsic property of the volume conductor leading to variations in the measured bio-impedance. Although the body is a closed loop and the extra cellular total fluid volume in a constant, redistribution causes regions of high fluid accumulation and regions of low fluid accumulation. These variations manifest in the bio-impedance signals as offsets and hinders true reproducibility of measurements [21].

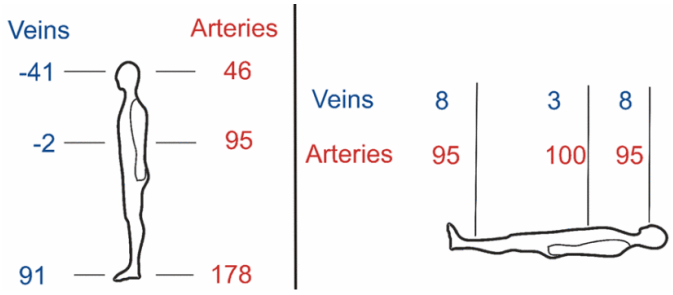

Figure 2.7: Illustration of the difference in arterial and venous fluid pressure(mmHg) between sitting and lying down. Source:[20]

2.3.3 Electrode Configuration for Measurement

Traditionally bi-polar measurement system configuration was popularly used. In this system, the current is injected into the load impedance network (human body) through two electrodes and the response voltage is measured by determining the voltage drop across the load through the same electrodes as shown in Figure 2.8. Consequently the ratio between the measured voltage and injected current would determine the impedance. This measurement set-up is simple and requires no extra hardware components and connections. However the voltage measured with this setup is not only across the load impedance but also includes the series electrode-skin impedances and contact impedance thereby miscalculating the impedance of the load [22].

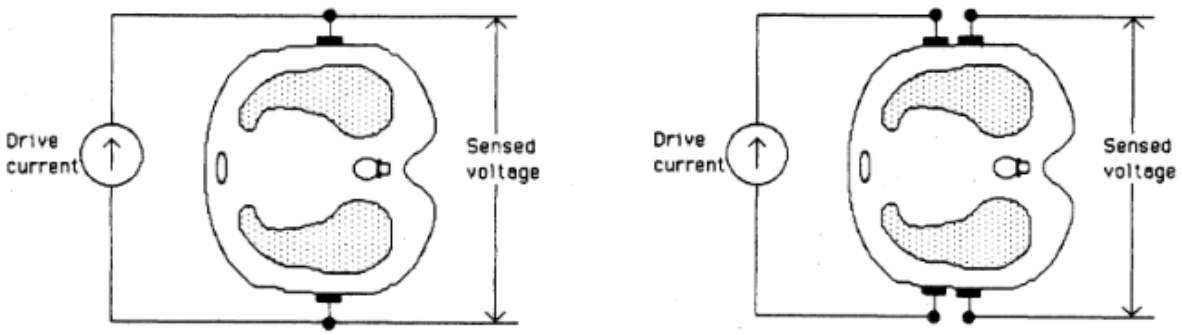

Figure 2.8: Left: Bi-polar Electrode Configuration Right: Tetra-polar Electrode Configuration [22]

To overcome this limitation, the tetra polar configuration was developed and is widely used [23]. In this set up two pairs of electrodes are incorporated and each pair does a separate task as shown in Figure 2.8. The current is injected into the load (human body) with one pair and the other pair is used to measure the voltage across the load. In addition, the electrode pair that measures the voltage offers high input impedance to limit the flow of stray current into the amplifiers. As a result, the voltage drop measured is only across the load.

2.3.4 System Requirements

The performance of a bio-impedance system is dependent on environmental and physiological states as described in the previous section. In addition, the performance of the systems is also dependent on technical reliability and errors that arise due to type of technology or components used.

The general architecture of a bio-impedance recording system is shown in Figure 2.9. On a system level, we recognize the signal generation unit and the signal recording unit as two main electronic intensive units.

Although each of the subsystems can be realized in numerous ways, each of these subsystems must observe certain general requirements to faithfully measure of bio-impedance signals. The objective of the following section is to highlight the general technical requirements of the two subsystems specifically for bio-impedance to reduce the errors in measurement and for its sustenance in the clinical setting .

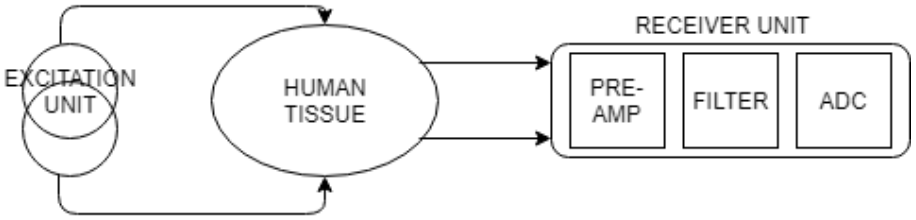

Figure 2.9: Representation of an idealized bio-impedance measurement system

Fundamental Configuration for the Recording Unit

The signal recording unit is probably the most challenging unit in the system. The unit should be able to truly pick up the required signal and discard the noise and artifacts. Reviewing the requirements of this unit will provide an insight into potential sources of common mode and noise related measurement errors.

During the measurement procedure, a potential is generated across the recording electrodes and the ground due to stray currents.This manifests as a common mode signal at the measurement input. It is vital for the amplifiers in the measurement unit to have maximum common mode rejection and minimal differential rejection [25]. In addition, common mode errors are also introduced due to the imbalance in the excitation current sources. The offset current will generate a voltage between the inputs of the measurement amplifier. A common approach across systems is the utilization of symmetric differential sensing amplifiers with high common mode rejection ratios with matched component pairs to reduce the effects of common mode errors [24].

The physically available analog signal is converted into the digital domain using analog to digital converters. The converters need to be efficient in-terms of power consumption, conversion time and resolution. In this context, the resolution is most critical because even a 20% change in hematocrit is a predictor for circulatory shock during plasma leakages [26]. Successive Approximation Registers and Dual Slope ADC's have the best performance in this regard [27]. In addition, ADC's are designed to oversample the acquired signal to increase the dynamic range and signal to noise ratio.

Excitation Unit

In general two basic approaches have been followed to design the excitation unit. It has either been voltage controlled or current controlled systems [28]. In a voltage controlled device, the excitation unit applies a potential difference between two points in the volume conductor and the current flowing between the two points is measured by the receiver unit. In a current controlled device, the excitation unit injects a constant current into the volume conductor and the potential drop along the conductor is measured by the receiver. In both these devices, the impedance is measured in accordance to ohm's law as shown in Equation 2.5, where f is the frequency of introduced electrical signal, V and I are introduced or measured electrical quantities depending on the type of device.

$$Z(f) = \frac{V(f)}{I(f)} \tag{2.5}$$

However, current controlled devices have been considered more often than the voltage controlled device to ensure that the current flowing through the tissues is constant throughout the procedure and not dependent on the changes in body impedance. This feature also doubles as a safety feature.

The excitation unit has to conform to IEC6061 standards. This standard has set a regulatory limit on the strength of the electrical signal applied to the body (500μA at 50kHz) to restrict the injected current within the water limit. It is also vital to ensure that the amount of DC current entering the body is less than 10μA [29].

It is therefore vital to consider these requirements during the development phase to avoid issues during clinical experimentation.

2.3.5 Existing Technology and Performance

In the market today, the most popular bio-impedance recording devices are the BioPac system (BioPac Inc), Hydra 4200 (Xitron Technology) systems, QuadScan(Body Stat), Omron Healthcare and BIACorpus. These devices have been considered to be the most effective bio-impedance measurement systems at the moment. The systems are extremely effective (best performance) in controlled clinical environments. However the devices are quite bulky, expensive and inconvenient for continuous fluid status monitoring.

There are multiple analog front ends available which help optimize system development in terms of both power requirements and size. AFE4300 is an analog front end by Texas Instruments that allows the development of multi channel recording systems with multiplexers but is limited by the bandwidth and frequency range for measurements [30].

On the other hand AD5933/AD5940 by analog devices is a promising alternative with wider bandwidth, programmable gain setting and larger measurement frequencies. Additionally various laboratory specific ASIC [44] and FPGA's have been developed, but none of them have made it through clinically [31].

The development in technology has allowed multiple strategies to measure and implement several bio-impedance recording systems. Several studies have been conducted comparing the mathematically estimated body composition parameters like TBW and fat free mass between the developed and reference devices. However there has been a rise in clinical interest with the utilization of raw bio-impedance values to characterize clinical conditions. The following section reviews the performances of devices presented in literature in terms of the raw bioimpedance values.

Performance of Existing Devices

The behavior and estimation of raw bio-electrical parameters like resistance, impedance, phase angle and reactance are clinically significant to track fluid shifts in patients.

The overall opinion suggests that two commercial devices can't be used interchangeably to measure the raw values due to performance variations linked to the technology and components used to develop the device. Therefore no single bio-impedance device has been marked as a reference gold standard.

The method of estimating the raw values vary between devices. A few measurement devices measure impedance and phase and then determine the values of resistance and reactance through trigonometric equations, while other devices measure the resistance and reactance first and then calculate the phase angles and impedance. As a result a variability in measurements is observed [32]. Phase angles measured by [33] using the Xitron and RJL-101 device show significant differences. The phase angles were constantly under estimated and varied as $-1.5 \pm 0.24^{\circ}$. This difference was considered to be appreciable and significant.

Similarly the determined reactance value between the devices Xitron 4200 and RJL varied significantly in [34]. The study reported no statistical difference with the resistance measurements with a t-test, however a bias of 3.82Ω was obtained. The limits of agreement presented was ±16Ω. Results obtained from study [35] showed that although there was a high association between the measured values the standard estimated error was 9.91Ω for resistance and 0.42° for phase angle. The reported width of limits of agreement was 60.7Ω for resistance,0.9° for phase angles. From the findings, it was not conclusive if the devices measured the same raw values on an average.

Despite the high association and agreement between two devices, results in literature showed large variations during individual measurements. A research prototype developed by [36] was compared with BCM-Fresenius device. The results suggested desirable association between the measurements through a high correlation r=0.99 and $p<0.001$, bias of 1.3Ω and a standard deviation of 2.1Ω.The values measured by [37] reported accurate measurement for SFB3 and Xitron devices when tested with impedance networks, however when tested for intensive care patients the measured values reported significant differences. With whole body bio-impedance devices that are not based on the phase sensitive principle, the measured error of impedance is 6% as reported by [38]. A common effect seen in literature is that errors measured at any individual frequency is minimized by the modelling and averaging effects[39]. The errors with modelling was more proficient for higher frequencies.

The device developed in [40] was very accurate with 0.05Ω error for impedance and 0.003° error for phase with a dynamic range of 100-1.1kΩ. With devices developed specifically for segmental bio-impedance the ranges reported are 0-345Ω by [41] and 32-5.3kΩ by [42]. The error of the former device was 3.9% for resistance and 6% for reactance. However a drawback of these studies is that apart from [41] the devices were not tested on human subjects and were only validated as bench top designs.

2.4 Motion and Positional Awareness

As stressed previously, bio-impedance measurements are susceptible to movement related artifacts and postural orientation. Eventually, measurement systems need to be robust and should have the awareness to identify instances related to motion.

In the past there have been several occasions where movement related contexts have been detected for similar purposes that aid in motion related noise cancelling, activity and position identification. Most of the mentioned approaches utilize body worn inertial sensors. Recent advancements in sensor technology has allowed the development of precise and affordable systems with inertial sensors. The review in the following sections will be focused specifically on accelerometers for activity and position detection given their size, cost and performance.

A standard approach followed during activity or positional classification involves at first, splitting the received signals into small time segments that can capture the essential features. Generally, two types of windowing techniques are popularly incorporated. Sliding windows are those that divide the signal into equal smaller window segments with no inter window gaps. The approach is simple and requires less sensor signal pre processing compared to other techniques. Context specific windows are used to define specific events. Pre processing is essential to identify specific contexts. These contexts are further used to define consecutive segments [43].

Movement generates certain patterns in the accelerometer signal. A number of features can be identified to quantify the magnitude of the patterns. Time domain features such as variance, mean and standard deviation are popular in the literature. Combination of acceleration moving variance detector and moving mean detector have been utilized by [45] in order to recognize movement contexts during EBI measurements. A leave one out cross validated SVM model was used and an accuracy of $97.4 \pm 2.6\%$ was reported using these features. Signal magnitude average (SMA) is another feature used to identify activity. SMA computes the acceleration under the time curve after removing the gravitational component. These features have been used by neural classifiers [46] and decision trees [47] without any major difference in accuracy (> 95) to perform activity classification.

Features can be extracted in the frequency domain as well. Average spectral entropy and energy is calculated to discriminate patterns of inactivity and activity. Results by [48] reported an accuracy of 92% when spectral entropy was incorporated in decision tree topology. Alternatively, a number of reports have also suggested the utilization of time-frequency features. Human activity detection was performed by [49] using wavelet features. The average recognition results for the activities was 95.45%. For positional orientation detection - along with accelerometers, gyroscopes have been employed to develop advanced body position algorithms [50] using sensor fusion. However, in this context there is no specific requirement to determine subtle position orientations as demanded by certain kinematics and gait related applications. In this context gross body positional changes such as sitting-standing-sleeping(laying down) need to be determined. For this purpose, simple tilt based algorithms can be used which measures the angles between the axis of the accelerometer and gravity.

Finally, the choice of the feature extracted and classification scheme depends on the computational power of the chosen hardware platform. The computational requirement of features extracted in time-frequency domain and frequency domain is higher than time domain. Similarly, a threshold based classification scheme has a low degree of complexity while advanced algorithms such as support vector machines and neural networks have higher computational complexity. On the other hand it is also important to appreciate the advantages offered by advanced algorithms as compared to simple thresholding such as generalized classification algorithms without the need to update thresholds based on inspection or the requirement of lengthy pre-processing steps.

Contextual Monitoring Applications

Sensor networks and distributed computing have shown that it is possible to develop devices that are aware of its surrounding based on contexts. An example of its capabilities are seen in the field of robotics and augmentation where positional and visual contexts help create a digital landscape of the surroundings. A similar approach can be incorporated by wearable health devices to construct motion aware systems.

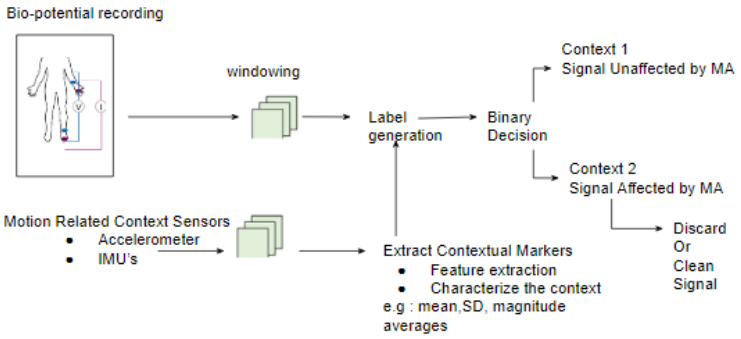

Figure 2.10: A conceptual illustration of a contextually aware bio-measurement systems

Motion sensing(activity and orientation) in the spatial dimension is of particular importance in the frame of this work. Most available motion sensing applications are derived from sensor integration into mobile systems. Accelerometers and gyroscopes have been used together to develop systems that are motion aware. Researchers in the field of biomedical engineering have also used sensor integration in their work to develop contextually aware devices. A dual classifier context algorithm was developed to extract pulse feature in the context of motion in the work undertaken by [51]. Applications such as this gives an insight into the circumstances of the measured physiological signals and helps the medical care-givers to make inferences based on interconnected references. Motion related artifacts are quite a relentless issue in all bio-signals. Inertial measurement units and sensor integration have allowed the estimation of the relative positions of the individual with respect to an iteratively adapted motion frame. This information has been further used to cancel the artifacts present in the biological signals measured [52]. A conceptual illustration of a contextually aware bio measurement system is shown in Figure 2.10. In [53] the awareness of the algorithm enabled the researchers to extract not only activity related information for adaptive motion artifact removal but also enabled them to make diagnostic decisions related to cardio-vascular disorders. The element of context builds abstractions of the ever changing situations around the system and will support in the development of smart systems, however the contextual cues extracted and the framework developed to flag the contexts is application specific. Additionally the computational resources required to implement such systems are higher and efficient classifiers and learning models will help reduce this burden.

2.4.1 Research Question

The limitations of the existing bio-impedance devices was previously mentioned. The performance of a bio-impedance measurement system is also sensitive to the environment of measurement, technical factors and physiological state. A new prototype device is developed in this work that can compensate for the mentioned factors. However it is required to assess the validity of the developed device before it can replace an existing commercial device in the clinical setting. To that extent, this work looks to test the performance of the developed prototype device against the commercial device with the following research questions

- Does the developed prototype bio-impedance system and the reference system measure the same impedance and reactance on an average?
- How repeatable and precise are the values measured by the prototype device compared to the reference system?

In addition to the above question, the work undertaken also proposes a methodology to enable the detection of activity and position to develop a motion aware system that can potentially compensate for the effects of postural variations and effects of motion artifacts in the subsequent development stages.

Chapter 3

Materials and Methods

3.1 Prototype Design for Evaluation Study

To address the objectives of the proposed work an experimental study was setup at Balgrist Campus AG, Zurich. The device used to perform the bio-impedance measurements was developed in house at the Mobile Health Systems Lab. Figure 3.1 illustrates the system level block diagram of the prototype system (AMBICA V2.0).

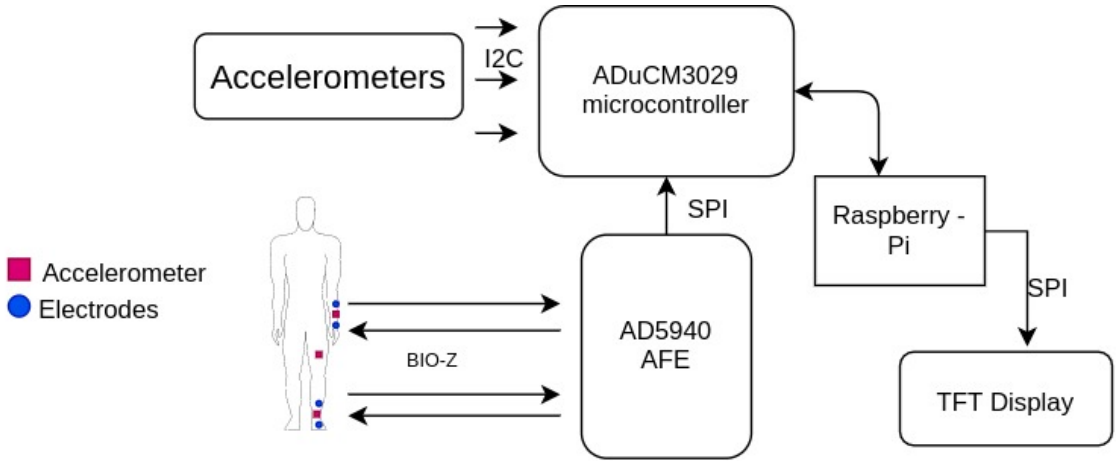

Figure 3.1: System Level Block Diagram of AMBICA V2.0.The placement of three accelerometers and electrodes are shown as well.

3.1.1 Bio-Impedance Sensor

The heart of the prototype that performs the bio-impedance measurement is the AD5940 (Analog Devices Inc) sensor. AD5940 is a highly precise analog front end (AFE) system designed to measure the response to an electrical excitation. The analog front end has configurable excitation loops and measurement channels operating from 3.3V supply.

The sensor AD5940 is in communication with the EVAL-ADuCM3029(Analog Device Inc) micro-controller development board through the serial peripheral interface (SPI) protocol. The micro-controller is utilized to configure the sensor digitally to allow 4-wire whole body bio-impedance measurements. AD5940 has a configurable excitation source with a high speed digital to analog converter (DAC) and waveform generator. The waveform generator is configured to feature a sinusoidal wave with a maximum output voltage of 1.2V (peak to peak). A current limited resistor is set at 1kΩ to limit the alternating current (AC) entering the human body to a maximum of 400μA (rms). In addition the AFE is configured to perform the measurements from 1kHz-100kHz with 1kHz increments at a rate of 20Hz. A 8192 sample discrete fourier transform is performed on the measured signal by the DFT accelerator to determine the real and imaginary components of the bio-impedance.

3.1.2 Accelerometer

MMA8451Q 3 axis digital accelerometer is used to measure the acceleration data with respect to movement and positional changes. The accelerometer communicates with the ADuCM3029 micro-controller through a inter integrated circuit (I2C) interface. The sensor is configured to measure the acceleration at 2g dynamic range with a resolution of 14 bits. The data is measured at 30Hz. The device is operated from a supply voltage of 3.3V.

3.1.3 Data Recording and User Interface

To ease the experimentation procedure a user interface(UI) was developed using a Raspberry Pi 3B+ (Raspberry Pi)and the Tkinter(Tcl/Tk) framework. The interface controls the entire sequence of operation from storing the entered study details and participant credentials to shutting the device down. The interface is accessed either locally through a virtual network computing(RealVNC) client or the 320x240 2.8" Adafruit PiTFT touch screen.

The UI controls the initiation and termination of bio-impedance measurement through the general purpose input output (GPIO) pins on the raspberry-pi connected to the ADuCM3029. Two GPIO connections are used specifically- one to reset the ADuCM3029 (resets the bio-impedance and accelerometer recording) and another to initiate the bio-impedance and accelerometer recording. The data recorded from the sensors is transmitted from the micro-controller to the raspberry-pi by accessing the serial port through a USB cable. The received data is stored in the memory of the raspberry-pi as text files.

3.1.4 Electrode and Accelerometer Placement

Placement of Electrodes

The 4 wire tetra polar bio-impedance measurement configuration was implemented. The electrodes (EL500 BIOPAC Systems Inc) are placed on the subject as shown in Figure 3.2 after thoroughly cleaning with ethanol (Braun Medical). The sensing electrodes were placed at the wrist and ankle while the source electrodes were placed centrally on the metacarpals on the palm and metatarsals on the feet. The electrodes are connected to the measurement device using long ECG cables with touch proof connectors mounted on the 3D printed casing. For all subjects, the electrodes were placed on the right limb.

Figure 3.2: Left to Right.1-2 : Placement of Electrodes , 3-5:Placement of Accelerometers

Placement of Accelerometers

Three accelerometers are used to faithfully reproduce movements that represent motion artifact signals and positional orientation. Two out of the three accelerometers are placed on the wrist and ankle (adjacent to the sensing electrode) with the Z axis oriented in the downward direction and the other accelerometer is placed on the quadricep region of the thigh with the Z axis oriented in the downward direction as shown in Figure3.2. The wrist-ankle accelerometer pair help to faithfully reproduce movements that represent motion artifacts in the bio-impedance signals while the thigh-ankle accelerometer pair help determine the posture of the subject. The accelerometers are enveloped in a rubber heat shrink and fastened using velcro. The accelerometers are connected to the device using a 4 core wire and 4 pole binder adapters mounted on the device casing.

3.2 Experimental Study and Protocol

3.2.1 Experiment - 1 : Pilot Validation with RC networks

A preliminary study was performed to evaluate AMBICA. A purely resistive network of 660Ω, one purely capacitive network of 1uF equivalent capacitance and a 2RC network (illustrated in

Figure2.2, Re = 550Ω, Ri=100Ω and C_m=1μF) was chosen and the impedance was measured from 1kHz to 100kHz. For each measurement the average absolute error was calculated. The reference values for the resistance and capacitance was estimated through laboratory digital multi meter, while the 2RC network was validated after performing a SPICE simulation.

3.2.2 Experiment - 2 : Healthy Volunteer Study

The experimental study was undertaken at Balgrist AG, Zurich and the study was approved by the ethics committee of ETH Zurich (EK 2018 N 69). Fourteen healthy volunteers were recruited for the study. The criteria for inclusion were age > 18, no existing skin disorders or allergies, no metallic or electrical implants, no pregnancy and failure to provide informed consent.

Preparation of Subject

Participant anthropometric data is collected at first like age and sex. Additionally, the participant's body weight, height, arm length and circumference, leg length and circumference is measured. Following the collection of anthropometric data, the electrodes and accelerometers are secured onto the body as previously mentioned and the subject is requested to lie down in a supine position as shown in Figure 3.3 for at least 5 minutes before performing the measurements to stabilize the hydrostatic pressure acting on the column of fluid in the body.

The experimental protocol will follow through as stated below and is specific in its objective.

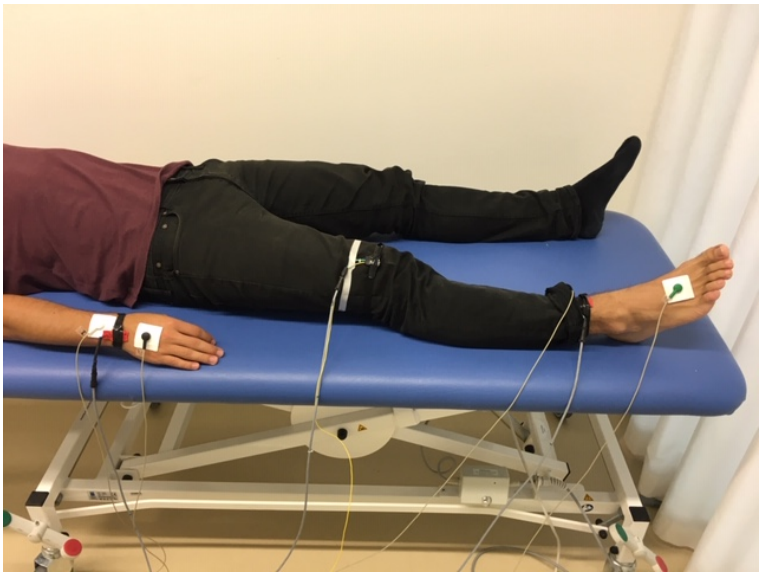

Figure 3.3: Participant in Supine Position

Measurement Protocol for Assessing Performance of AMBICA

While in a supine position, three consecutive measurements are performed alternatively between the reference device(BIACorpus) and prototype device. One set of measurement involves recording with BIACorpus followed by the prototype device for 30 seconds.

Measurement Protocol for Generating Periods Affected by Movement Artifacts

The whole body bio-impedance (frequency sweep between 1-100kHz) and data from accelerometer is measured using the prototype device. During the measurement the participant is requested to perform certain specific movement related tasks as listed below while lying down.

- wrist rotation
- arm rotation
- movement of arm up and down
- ankle rotation
- leg rotation
- movement of leg back and forth
- rotation of body on the bed

The sequence of recording for a single movement related task is as follows and is designed to introduce movement related artifacts during measurements.

- 30 seconds of supine without movement
- 60 seconds of one movement related task
- 30 seconds of supine without movement
- 60 seconds of the same movement task
- 30 seconds of supine without movement.

  The total time taken to complete one sequence is 3.5 minutes seconds and this is performed seven times altogether (for all movements) and hence the total experimental time is around 25 minutes.

Measurement Protocol for the Determination of Body Postures

The whole body bio-impedance (frequency sweep between 1-100kHz) and data from accelerometer is measured using the prototype device. During the measurement the subject is requested to perform certain specific positional tasks as listed below.

- Supine
- Sitting
- Standing

The sequence for measurement is as follows and is designed to obtain the transition between each position as well as to ensure that the impedance signal stabilized within that period.

- 40 seconds laying supine
- 40 seconds siting upright
- 40 seconds standing upright
- 40 seconds sitting upright
- 40 seconds laying supine
- 40 seconds standing upright
- 40 seconds laying supine

The total time taken to complete this sequence is 280 seconds.

3.3 Data Analysis

The data recorded from the reference and prototype device was uploaded into the database for further analysis using MATLAB(R2016b Mathworks Inc).

In this thesis magnitude of impedance (also referred to as just impedance in the report) is referred by the Equation 3.1 and reactance (Xc) is assessed as a positive vector as the data recorded from the reference device measures Xc as a positive vector on the imaginary axis.

$$|Impedance| = |Z|(\Omega) = \sqrt{R^2 + Xc^2} \tag{3.1}$$

3.3.1 Comparison between Reference Device and AMBICA

Bio-impedance measurements from AMBICA was compared with BIACorpus reference system. For the sake of this study the measured values from BIACorpus are considered as reference value even though the device has it's own error tolerances.

Test for Association

- Pearson Correlation : Utilized to assess the association between the devices and to indicate the the presence of a linear relationship between the devices. The correlation coefficient 'r' ranges between [-1,1]. r=0 indicates absence of a linear association while r=$\pm$1 indicates the presence of a linear association in positive and negative direction respectively.
- Error Metric : Root mean squared error(RMSE) was calculated between the measured values for each subject across the an entire frequency sweep. RMSE was calculated as using Equation 3.2.

$$RMSE(ohm) = \sqrt{\sum_{i=1}^{n} \frac{(referencevalue - measuredvalue)^2}{N}} \tag{3.2}$$

Test for Agreement

Bland altman plots are presented to compare the performance between the device. The difference of measured values in Ω is plotted against the mean of the measured values. The bias, standard deviation of difference(sd), limits of agreement and confidence intervals for bias and limits of agreement were calculated. The limits of agreement is computed after testing for normality of the difference in measurements using the Anderson Darling test for normality at 5% significance level. The 95% limits of agreement is calculated as b$\pm$1.96*sd. Regression based confidence intervals is calculated for those instances where there is trend between the difference and mean values.

The coefficient of error (CE) is calculated as $\frac{SD}{M*sqrt(n)}$. The precision is considered as 2*CE [54]. A low CE score suggests higher precision and low dispersion of data points.

3.3.2 Framework for Activity Classification and Position Determination

To determine periods of activity and orientation of position the framework shown in Figure 3.4 has been followed. The length of window chosen is 20 samples with a 50% overlap between the windowed segments. The x, y, & z axis outputs from each of the accelerometers are filtered using a lowpass filter with a cutoff frequency at 3Hz.

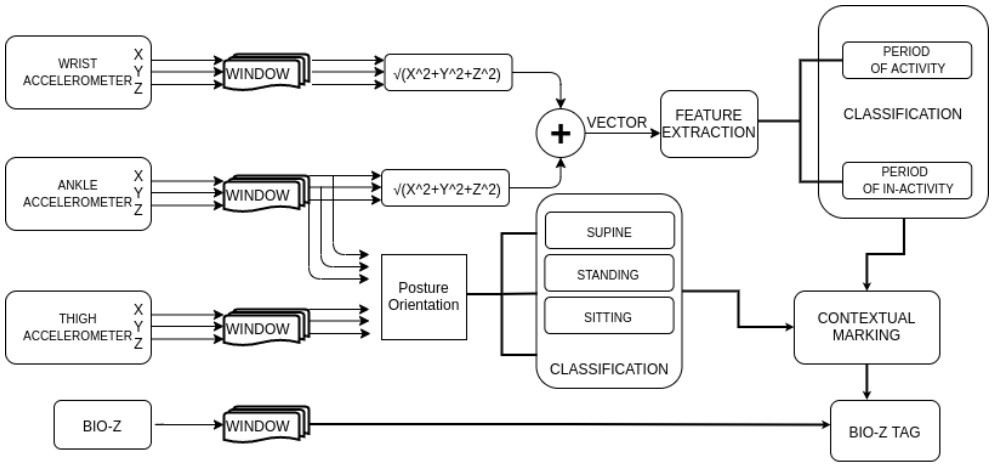

Figure 3.4: Framework for Movement and Position Awareness

A resultant vector from wrist and ankle accelerometer data is calculated and combined to form a single vector for activity classification. The features extracted from the vector for activity classification are the the normalized spectral entropy as described in equation 3.3 where $P(\omega_i)$ is the normalized power spectral density and and moving standard deviation where the standard deviation of signals within the window is calculated. For the determination of body posture the cosine of the z vector is calculated for ankle and thigh accelerometers as described in Equation 3.4.

$$PSE = -\sum_{i=1}^{n} * \frac{P(\omega_i)}{\sum_i P(\omega_i)} * ln(\frac{P(\omega_i)}{\sum_i P(\omega_i)}) \tag{3.3}$$

$$\theta = \arccos \frac{a_z}{\sqrt{a_x^2 + a_y^2 + a_z^2}} \tag{3.4}$$

The data from the upper and lower leg accelerometer pair were used to identify the angles associated with the body postures. Posture classification was performed using a decision tree. Data was divided into a training (8 subjects) and a hold-out test set (2 subjects). Ten models were trained using cross-validation with class balancing before training. The model with the least validation error was selected.

The metrics used for evaluating the model are Accuracy, Sensitivity and Specificity.

$$Accuracy = \frac{TruePositive + TrueNegative}{TotalPositive + TotalNegative} \tag{3.5}$$

$$Sensitivity = \frac{TruePositive}{TruePositive + FalseNegative} \tag{3.6}$$

$$Specificity = \frac{TrueNegative}{TrueNegative + FalsePositive} \tag{3.7}$$

Chapter 4

Results & Discussion

4.1 Participant Demographics

An overview of participant demographics is presented in Table 4.1. A total of fourteen healthy participants were recruited for the study. Eight females and six males were involved in the study. Eleven of the fourteen participants were from a European ethnic background, two participants were East Asians and one participant was South American. For the study to compare the performance of the developed prototype, four participants were excluded. One due to a technical failure during the measurement with the prototype and three due to failures with the reference device. For the study that involved determining the motion period and postural orientation, one participant was completely excluded due to a technical failure during the measurement. For specific experiments involving ankle rotation, leg rotation and body rotation two participants were excluded, for leg motion three participants were excluded and for body postural changes one participant was excluded due to poor data recording. The demographics details are presented as mean $\pm$ standard deviation.

	Male (n=5)	Female (n=9)
Height(cm)	179.633 $\pm$ 7.7089	163.187 $\pm$ 4.4315
Weight(kg)	76.95 $\pm$ 9.8523	60.2625 $\pm$ 5.9037
BMI(kg/mˆ2)	23.84 $\pm$ 1.829	22.7250 $\pm$ 2.8263
Age (Median)	27	25.5

Table 4.1: Participant Demographics

.

4.2 Comparison of AMBICA In-Silico

Distinct RC networks were used to validate the prototype device prior to clinical tests. For each network the measurements were conducted from 1kHz-100kHz. The average absolute impedance error for the resistor was 0.437Ω and -4.512Ω for the capacitor network. The model RC network was compared with the SPICE simulated values. The average absolute difference of impedance measured was -21.5Ω.

4.3 Comparison Between Devices

The developed prototype AMBICA was compared against the BIACorpus reference device to analyse the measured impedance and reactance. Table 4.2 shows the maximum and minimum values recorded by both the devices. The range of impedance measured by BIACorpus is slightly higher but comparable to the range of AMBICA, especially when we consider the resistance measured during the pilot validation. AMBICA recorded a larger range (83.33 Ω) of reactance compared to BIACorpus (67 Ω).

	AMBICA	BIACorpus
Max Impedance(Ω)	627.2047	625.352
Min Impedance(Ω)	348.274	335.173
Range Impedance(Ω)	278.93	290.2
Max Reactance(Ω)	93.156	82.6
Min Reactance(Ω)	9.8212	15.6
Range Reactance(Ω)	83.3357	67

Table 4.2: Range of measured Impedance and Reactance Values

Figure 4.1 illustrates the general variation of magnitude of impedance with frequency. The mean of magnitude of impedance over three cycles is plotted against the frequency sweep. It can be observed that the magnitude of impedance (Z) decreases with increase in frequency for both devices. On an average AMBICA overestimates the impedance value with the exception of subject 1.

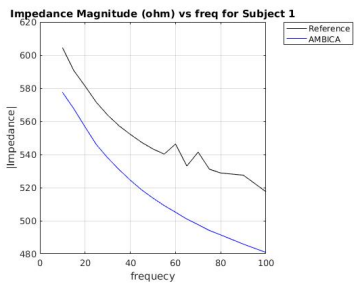

(a) Subject 1

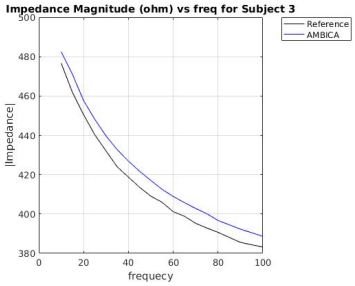

(b) Subject 3

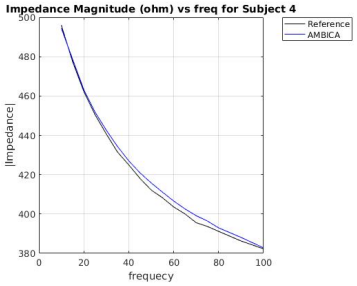

(c) Subject 4

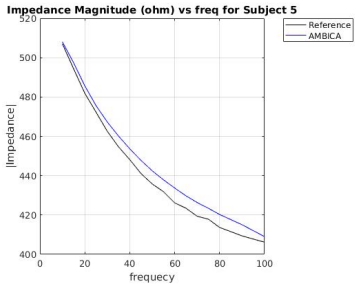

(d) Subject 5

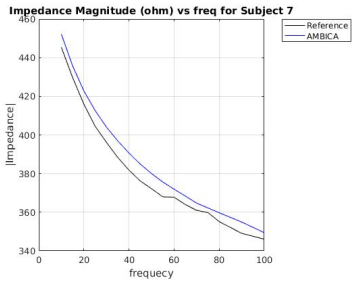

(e) Subject 7

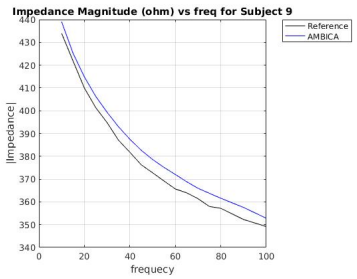

(f) Subject 9

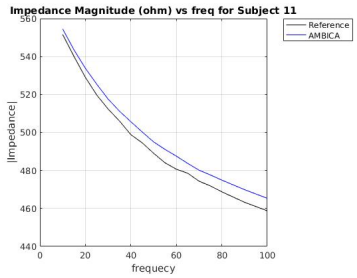

(g) Subject 11

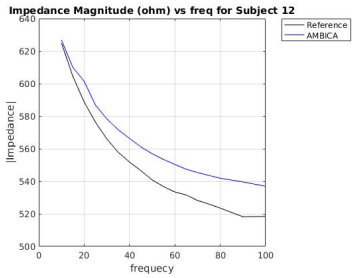

(h) Subject 12

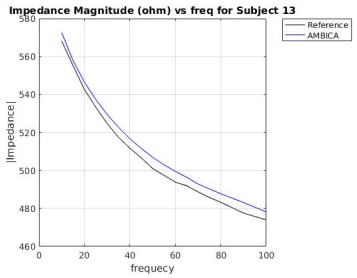

(i) Subject 13

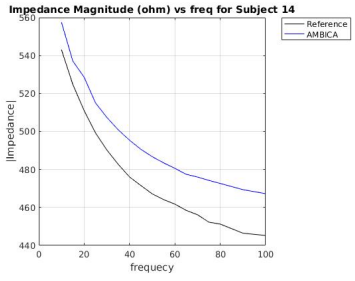

(j) Subject 14

Figure 4.1: Magnitude of Impedance (ohm) vs Frequency (kHz) plots generated for all 10 subjects.Blue Curve : Data from AMBICA. Black Curve : Data from BIACorpus.

Figure 4.2 shows the general trend of reactances between the two devices. The figures illustrates a reactance(Xc) vs Real(Z) plot. It is observed that both devices show a semi-circular trend similar to the typical R-Xc curve seen in Figure 2.5. As seen with impedance plots, reactance for subject 1 is overestimated while for the others it's been underestimated.

Figure 4.2(h) & 4.2(j) show that the measured value of reactance is negative for AMBICA. As stated in the previous chapter, the values for reactance are chosen as a positive vector. Therefore negative reactance values measured for this subject at higher frequencies is a technical error by AMBICA. This was observed with two subjects, subjects-14 & 12 and only beyond 60-65kHz.

The RMSE measured for the two quantities are shown in Table 4.3. The impedance value obtained from subject 4 was the closest to the reference value indicated with a RMSE of 2.001 Ω, while values obtained from subject 1 were the furthest away from the reference with a RMSE value of 31.705Ω. Similarly, the RMSE for reactance was maximum for subject 12 (44.98Ω) and least for subject 7 (9.29Ω).

Subject	1	3	4	5	7	9	11	12	13	14
Z - RMSE Ω	31.70	7.35	2.001	5.16	6.22	5.14	5.639	14.37	4.68	18.75
Xc - RMSEΩ	14.32	10.90	13.48	10.58	9.29	11.87	14.63	44.98	14.49	35.83

Table 4.3: RMSE for Z and Xc

Correlation between the measured impedance values suggest that there is a significant linear association with r>0.98 & p<<0.05 for all subjects. The correlation coefficients are all positive indicating the association is in the same direction as well. On the other hand the correlation between the measured reactance values between the devices indicate a weak correlation ($0.10 < r < 0.67$) for subjects 1,3,4,5,7,9 and 11. Correlations coefficients calculated for subjects 12(r=0.93,p$< 10^-10$), 13(r=0.70,p$< 10^-4$), 14(r=0.88,p$< 10^-8$) indicate a stronger correlation between the measured values. In addition, subjects 5 & 7 also showed a weak negative correlation (r=-0.04 & r=-0.11 respectively).

Figure 4.3 shows the scatter plot between AMBICA and BIACorpus for both impedance and reactance measurements for five subjects. The plots for the other five subjects are shown in Appendix A.1. The figures show a plot between AMBICA(y axis) vs BIACorpus(x axis) for impedance and reactance measurements. The plots show that the impedance values are densely distributed along the line of equality, while the reactance values are not deviated from the line of equality and the distribution is in fact sporadic. It can also be observed that the third impedance measurement cycle for subject 9 has been largely deviated from the line of equality owing to spurious readings from the reference device.

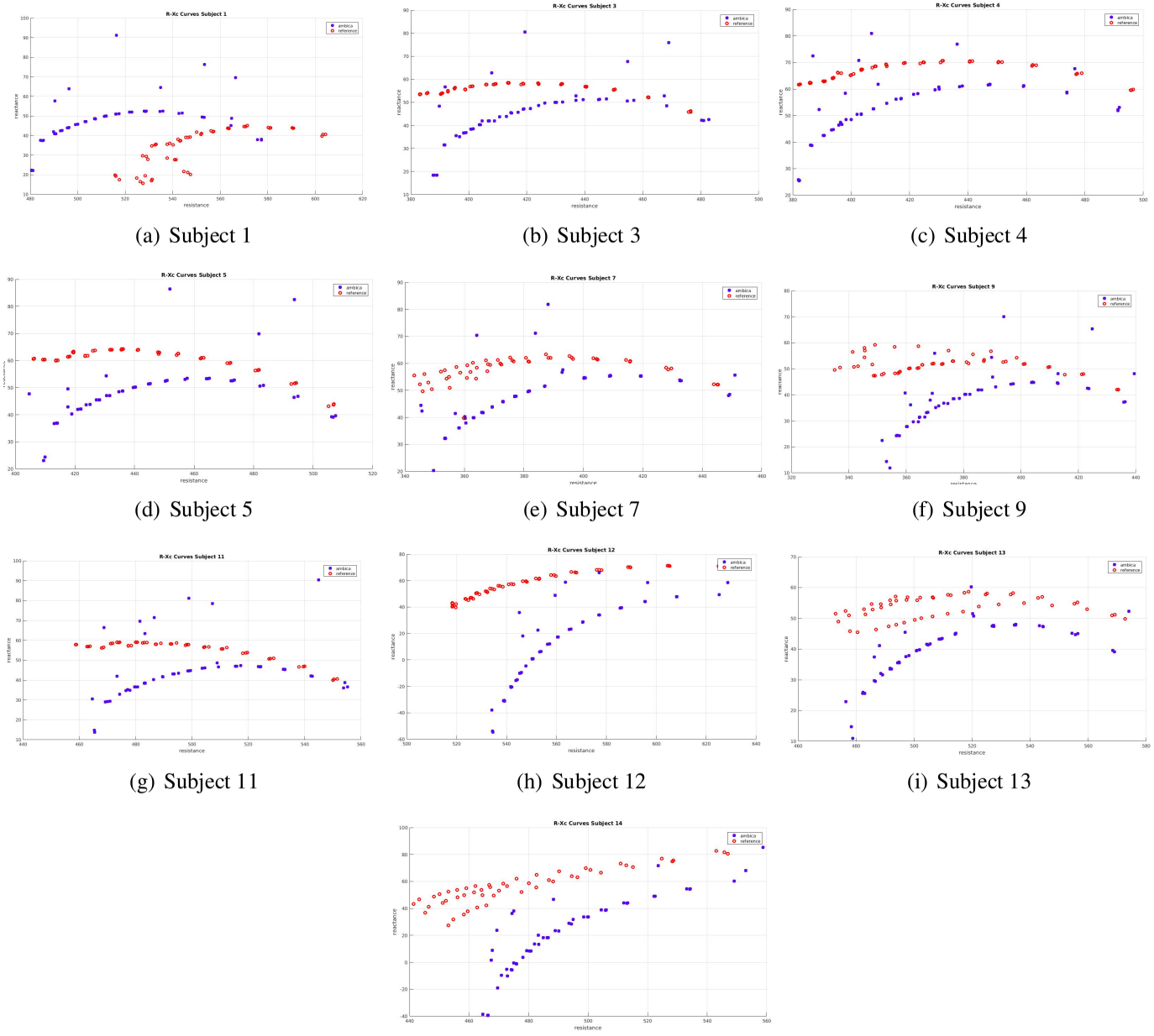

(a) Subject 1 (b) Subject 3 (c) Subject 4

(d) Subject 5 (e) Subject 7 (f) Subject 9

(g) Subject 11 (h) Subject 12 (i) Subject 13

(j) Subject 14

Figure 4.2: Reactance vs Resistance plot (Ω) – from right to left : increase in frequency.Blue Scatter : Data from AMBICA. Red Scatter : Data from BIACorpus.

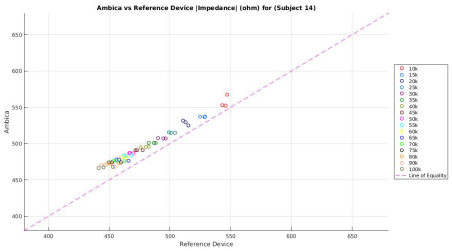

(a) Subject 14 Impedance Plot

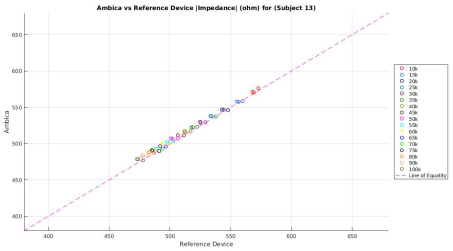

(b) Subject 13 Impedance Plot

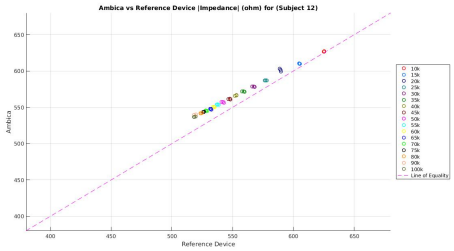

(c) Subject 12 Impedance Plot

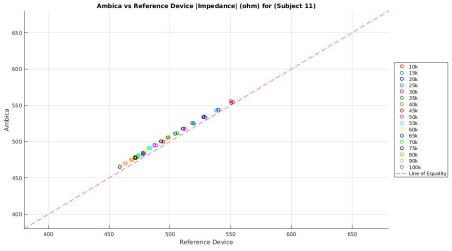

(d) Subject 11 Impedance Plot

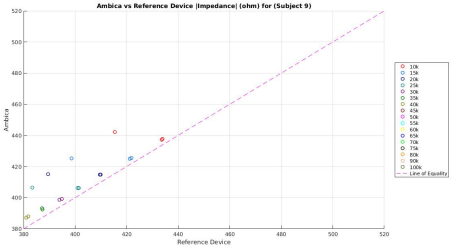

(e) Subject 9 Impedance Plot

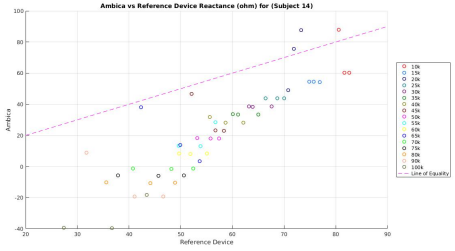

(f) Subject 14 Reactance Plot

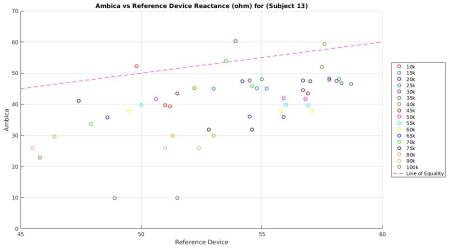

(g) Subject 13 Reactance Plot

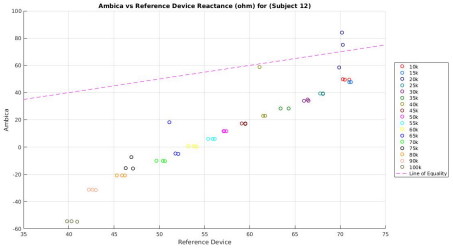

(h) Subject 12 Reactance Plot

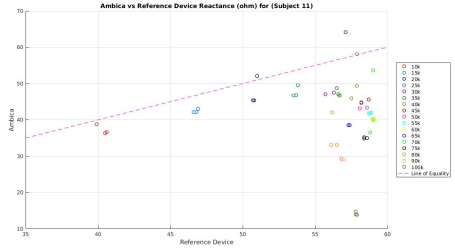

(i) Subject 11 Reactance Plot

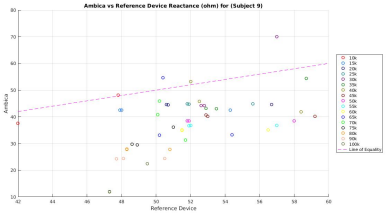

(j) Subject 9 Reactance Plot

Figure 4.3: AMBICA vs BIACorpus plots for impedance and reactance.Data Points at each Frequency is color coded.

4.3.1 Comparison as an Indication of Agreement

Figure 4.4 illustrates the bland altman(BA) plot for all subjects where the difference of the measured impedance is plotted against the mean of the measured impedance values. From the figure it is seen that the differences for subject 1 lie completely outside the estimated limits of agreement. It can also be seen that the measured pair-wise differences for subject 14 and subject 12 also have significant deviation. It is also observed that the confidence interval for the mean lies below the line of equality (y=0 line) indicating the presence of a significant negative bias. Only for subject 1 and a few individual differences for subject 4 & 13 have positive differences been encountered. From the BA analysis the bias and standard deviation is estimated as -4.50$\pm$13.01Ω, the limits of agreement are [21.0,-30.0]Ω and the width of CI for the mean is [-6.1,-3.0]Ω. For the cumulative plots, the average of three cycles of the reference device is considered as a reference reading. Subsequent plots in the appendix show the behavior for each cycle to highlight the variations found.

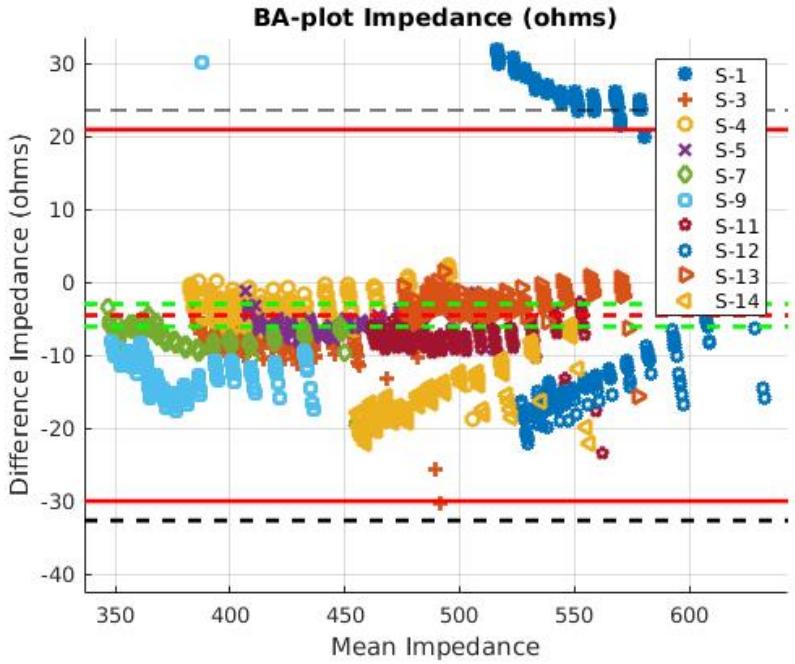

Figure 4.4: Cumulative BA plot for impedance measurements
The red dotted line indicates the bias, red solid lines indicate the limits of agreement (LoA), black dotted lines indicate the confidence intervals(CI) for LoA and green dotted lines indicate the CI for the mean.

Figure 4.5 shows the histogram of differences between the measured impedance. The large positive difference contributed by subject 1 is shown in far right of the histogram.

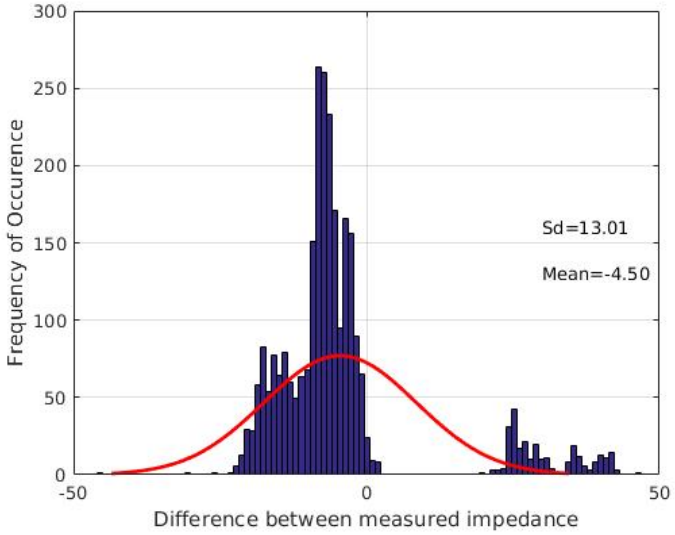

Figure 4.5: Histogram of difference between measured impedance.

Figure 4.6 illustrates the BA plot for all subjects where the difference of the measured reactance is plotted against the mean of the measured reactance values. From the figure it is seen that neither the CI for mean nor the LoA can envelope all the differences measured. The bias and standard deviation is estimated as $14.84 \pm 19.66\Omega$, the limits of agreement are [53.36,-23.68]Ω and the width of CI for the mean is [17.18,12.49]Ω. It is observed that the confidence interval for the mean lies above the line of equality (y=0 line) indicating the presence of a significant positive bias. An exception is that measurements from subject 1 consistently show negative difference during reactance measurements.

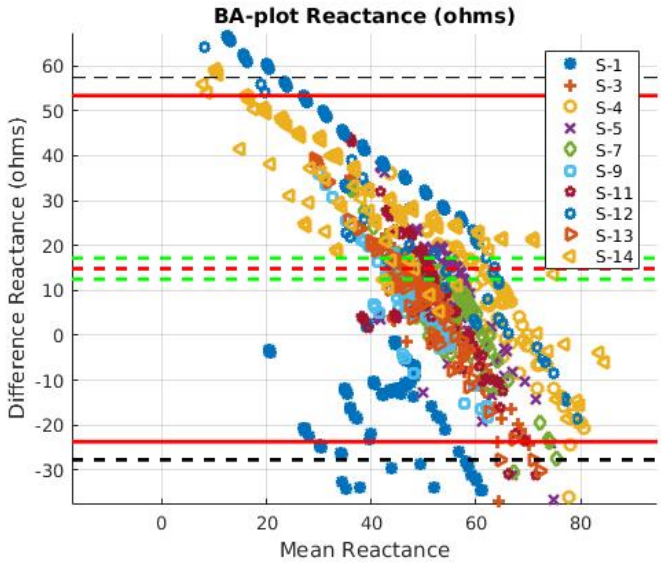

Figure 4.6: Cumulative BA plot for reactance measurements

Figure 4.7 shows the histogram of differences between the measured reactance. A spread of the differences is observed.

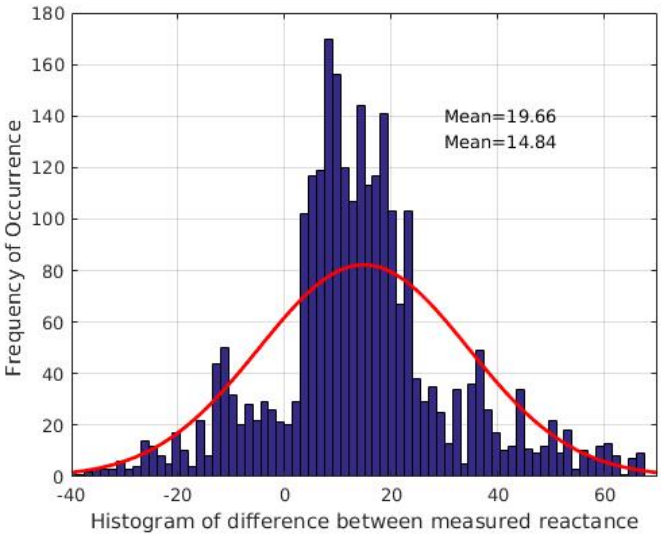

Figure 4.7: Histogram of difference between measured reactance

Table A.3.1 provides the average difference and variation statistics related to the differences observed during measurements at each frequency for all subjects. The table provides an insight into the differential behavior of the device at frequencies from 10kHz-100kHz.

Scores for Precision

Precision is estimated as 2*coefficient of error (CE) and is illustrated in Figure 4.8. For the impedance measurements we see that for subjects 9,12,13,14 AMBICA had considerably better precision compared to the reference device, while the precision during the measurements with subjects 4,11 were similar between the two devices. The reference device measured more precisely for impedance measurements with subjects 1,3,5,7. On the other hand the precision of AMBICA was much better for reactance measurements. As seen in Figure 4.8, the score for the reference device was consistently high(except subject 11,12) indicating a higher variation in the values measured. The precision score was comparable between the devices for subject 4 & 5.

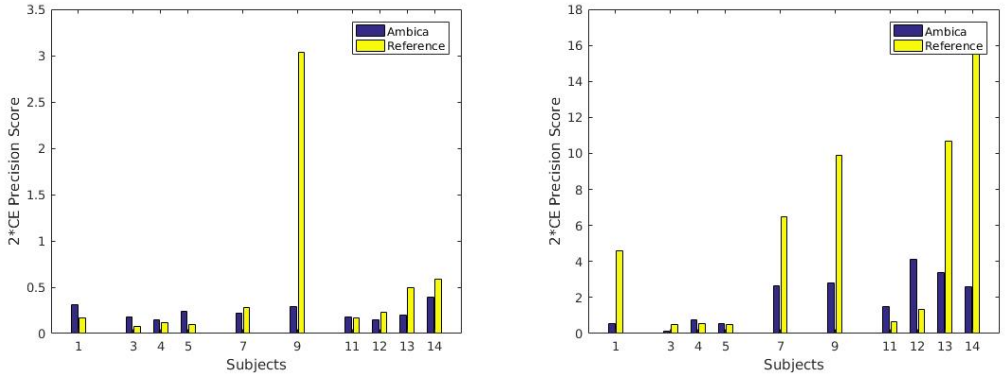

(a) Precision : Impedance Measurements (b) Precision : Reactance Measurements

Figure 4.8: Precision scores measured as 2*CE in % for impedance and reactance measurements The smaller the value the better the precision.

4.3.2 Discussion

Trends in the Raw Impedance & Reactance Measurements

Whole body bio-impedance measurement is the primary focus of this work. The range of values measured by AMBICA is in the range of whole body bioimpedance measurements. The range was highly comparable to BIACorpus. In that regard AMBICA has the ability to measure raw values in the typical range of whole body bioimpedance measurements.

The raw measurements of impedance and reactance showed two typical curves as expected from literature.

- The impedance values decreased with the increase in frequency. The tissues and cells in our body exhibit a differential behavior to low and high frequency current. As the frequency increases the impedance is expected to decrease (refer background Section 2.1). This trend was captured significantly by AMBICA. Figure 4.1 illustrates this trend.

- The R−Xc graph illustrated in Figure4.2 exhibits the typical semi-circular plot (refer Section 2.2.2). In-fact this trend is more prominent with AMBICA than with the reference device. The peak of the R−Xc curve marks the characteristic frequency f_c. At this frequency the current flowing through the intra cellular regions is equal to the current flowing through the extra cellular regions and is a critical parameter for fluid status monitoring. Previous research [55] approximates the presence of this peak at 50kHz (theoretically). Experimentally the presence of this peak is at 32kHz for males and 35kHz for females (median values). From the plots illustrated earlier, the peaks associated with AMBICA are between 35kHz - 40 kHz which is in line with previous findings.

The principal finding from this study suggests that the impedance values measured by AMBICA agree more closely with the reference device than the measured reactance values, within the bandwidth of frequencies considered for the bioimpedance measurements. In literature most developed bio-impedance systems have been validated with RC-networks. The dynamic range of the system developed by [40]was between 100-1.1kΩ with a 0.05Ω error in impedance measurements. Another device developed by[41] reported an error of 3.9% error of resistance and 6% error for reactance. The error measured in-silico with AMBICA was greater than error value reported by [40]. The error values obtained in this study (in-silico experiments) was comparable with [41]. Studies in [33], [34] & [35] all reported the presence of a significant systematic bias between the instruments used during clinical validation. Our device agreed more closely with the reference device for impedance measurements compared to the results from [35]. The bias estimated overall in this study was -4.50Ω and this is considerably lower than -9.91Ω as reported in the study. However, the study reported better agreement with the reactance measurements where the bias was -0.97Ω as compared to 14.84Ω from our study. It is important to take into account the vast differences in sample sizes in all the studies. The sample size has a large effect on the estimated width of the limits of agreement($\sigma/\sqrt{N}$).

Inter and Intra Subject Variation in Differences

A strong linear association was observed between the impedance measurements. Despite this, a significant discrepancy was observed between the measured values that varied largely. The isolated case where AMBICA underestimated the impedance value with subject 1 can not be explained with sufficient certainty. The smallest average difference for impedance measurements in any cycle was observed for subject 13 in measurement cycle three while the largest average difference was observed for subject 1 in measurement cycle 1. The standard deviation in difference although low for most subjects, SD was observed to be large for subjects 14,12 and 1 indicating a greater variability in the measured differences. The high variation in difference observed for subject 9 is due to erroneous values from the reference device as observed in the scatter plots. It was observed that the difference in reactance between the two devices is appreciably larger than that of impedance measurements. The variation in differences measured for reactance is much larger compared to impedance measurements, with a large standard deviation for all subjects.

Altogether, the differences between measured values were not similar between subjects for either AMBICA or BIACorpus. The differences however are quite similar across the three cycles for individual subjects for both impedance and reactance measurements. This type of variation was observed in [35]. The justification provided suggests that due to endomorphic variables, each human tissue has different morphology and as a result the recording system has a tendency to behave differently. This also includes factors such as the presence of dense tissue layers and variation in the levels of adipose deposition that attenuate the bio-electrical signal before it manifests at the surface. Since each subject has different compositions, the ability of the recording system to perform at optimal level is not maintained.

Trends in Bland Altman Plots With Frequency

The differences measured between devices increases as the frequency of measurement increases for both impedance and reactance. This is seen as a trend between difference versus mean in the bland altman plots for individual subjects. For the impedance measurements, this trend is observed for subjects 1,12,11,14,7,5 with correlation coefficient $r>0.65$, while for other subjects the effect is weak ($0.23 < r < 0.41$). Similarly, this trend is observed for all subjects with reactance measurements with $r>0.73$, especially beyond 35kHz. The agreement was stronger at lower frequencies than at higher frequencies. From the Table presented in A.3.1 it is seen that the increase in difference with frequency is more obvious for reactance measurements. To accommodate for this trend, confidence intervals using regression analysis were estimated for subjects where the trend was maximally observed as shown in the Figure A.2.

Precision of AMBICA

Repeatability of measurements is dependent on maintaining a constant measurement environment. With the controlled measurement settings in our study, it was possible to answer our second research question regarding the repeatability of the measurements. From Figure 4.8 we can observe that the precision and repeatability of AMBICA outperforms BIACorpus. This statistic can also be verified by the sporadic R-Xc graphs shown in the results. The limits of agreement estimated in this study are tight for impedance measurements and wide for reactance measurements compared to the devices mentioned in literature. The limits of agreement for impedance measurements reported by [34] was $\pm 16\Omega$, by [35] was -40.1Ω to 20.7Ω. The width of limits of agreement estimated from this study is [21.0,-30.0]Ω which is less tight than the former study but more tight than the result from the latter study. The limits of agreement for reactance measurements were however wider in this study compared to results from literature. However, from Figure 4.8 it is comprehensible that the variability in the measured differences was contributed majorly by the reference device than AMBICA. Under these circumstances the precision of AMBICA is appreciable.

Inconsistencies Observed With Reactance Measurements

R-Xc curves of both the reference and AMBICA showed several inconsistencies. For subjects 3,4 & 5- at higher frequencies the reactance values keep increasing without decreasing or decreased very slowly. This error was analyzed by [56] and provides an insight towards this discrepancy. The behavior exhibited is linked with the Hooke Effect due to parasitic capacitive leakages. For subjects 12 & 14 inconsistencies were observed with the data from AMBICA. The measured reactance values were negative beyond 60kHz. The premature tailing of the reactance past the characteristic frequency is observed due to inductive effects between long recording cables, contact impedances, imbalance of electrode-skin impedance and parasitics thereby inducing errors. These inconsistencies were also observed in [57].

Implications in the Clinical Scenario

The raw values measured like impedance and reactance are not in itself predictors of clinical conditions. The progression of dengue fever is marked by changing fluid quantities in the body. With the measured raw bioimpedance values biomarkers such as the impedance ratio can be estimated. Thus, the presence of a bias in the measured raw values may not affect the clinical utility. This would however mean that when going forward it is important to determine the significance of the bias present. Threshold bias and limits suggested by clinical members will also help to determine the range of acceptable values. Values measured beyond this limit would be disregarded for estimating the required diagnostic quantity.

However, this would require a thorough study of the range of acceptable values at each frequency and physiological conditions which is quite frankly a daunting task considering the number of inter related factors. The performance of AMBICA in clinical diagnostics will also be determined by the resolution of the device which has not been tested in this study. Ideally it would be desirable if AMBICA can significantly measure the smallest change in fluid volume. Evaluation on this front will challenge the technical performance of the various sub-systems present within AMBICA.

Limitations of the Study

- Number of Subjects Recruited : A number of inconsistencies are observed in this study. A large sample size would help assess these effects with greater certainty. Along with the large sample size, the performance of the device needs to assessed with wider ethnic population.

- Measurement Cycle : Three measurement cycles were chosen for this study. Increasing the number of cycles to ten will help with the estimation of repeatability and precision with more certainty. The estimated limits of agreement will also tend to be more tighter as multiple measurements are taken. Multiple measurements could be performed at least with the reference device as AMBICA has a faster recording rate.

  Increased measuring cycles and subjects will also allow fair comparison with the studies reported in literature.

- Range of Frequency Sweep : The frequency sweep range in this study was chosen between 10kHz - 100kHz, justified by clinical requirement. However, the behavior beyond these bands are unknown but contain valid information which is otherwise hidden. Wider frequency sweep will throw more light into how the measured values converge towards this range and how they diverge after this range. This will help to verify the presence of parasitics in the measurements which are more apparent at higher frequencies. The errors seen in R-Xc trends can be better explained with wider frequency sweeps.

- Contact Impedance and Proper Configuration of Electrodes and Cables : Errors due to loss of adhesion affects the proper placement and configuration of the electrodes and cables. This study did not have any method to verify the proper placement and connection of electrodes and cables. Utilizing the switching configuration of AD5940 it is possible to estimate the magnitudes of contact impedance through each measurement and current injection branches. Measuring these values prior to actual bioimpedance measurements will allow one to gain more insight towards the presence of additional contact impedance and improper fixation of electrodes.

- Lastly, the device was also not tested on dengue affected subjects. Results may vary depending on clinical condition. It will also further assess the agreement between the devices.

4.4 Motion Classification - Activity & Posture

A stride closer to intelligent bio-impedance monitoring would be to gather information regarding the movement and generating contexts of the measured signal.

4.4.1 Detection of Periods of Activity

Figure 4.9 illustrates the bioimpedance signal and corresponding z-axis measurement from the accelerometer during inactive and active periods during a measurement cycle. From the figure it is observed that the bioimpedance signal is highly susceptible to the induced motion.

It is also observed that within a given window the standard deviation and spectral entropy are good indicators of the presence of movement induced artifacts due to the high variations in the measured accelerometer signal during periods of activity.

Figure 4.10 illustrates the effectiveness of the features chosen to represent periods of activity and inactivity. Two exemplar plots are illustrated here and others are illustrated in Appendix A.3.2.

The outliers and long whiskers of the box plot are apparent due to the ineffective recording of time stamps during the experiment leading to improper label generation at the times of transition. As a result the outliers were removed before training the classification models. Table 4.4 presents the cumulative mean and median of the features extracted during active and inactive periods for all motion tasks.

	Spectral Entropy		Standard Deviation	
	Inactivity	Activity	Inactivity	Activity
Median	0.008	0.12	0.02	0.56
Mean	0.011	0.14	0.04	0.80

Table 4.4: Table presents the mean and median values for the features extracted for all motion related activities.

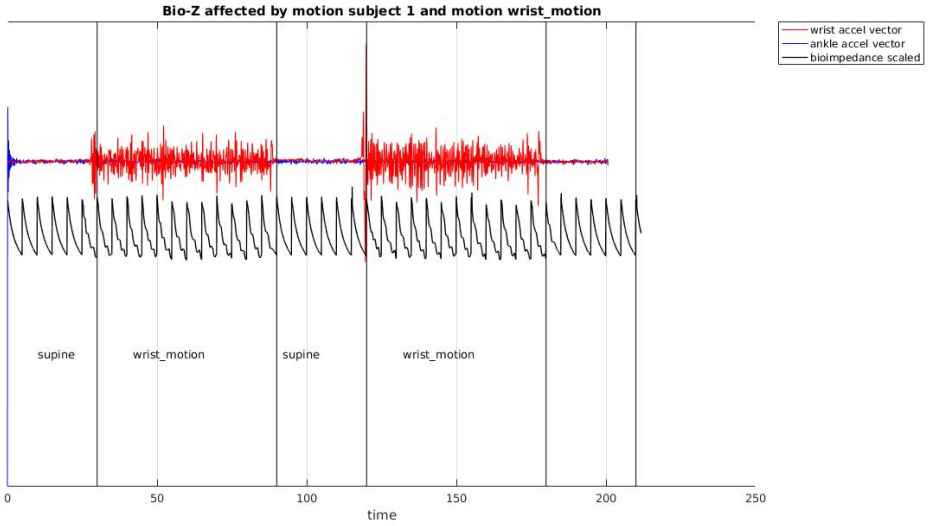

(a) Bioimpedance signal affected due to the movement of the wrist

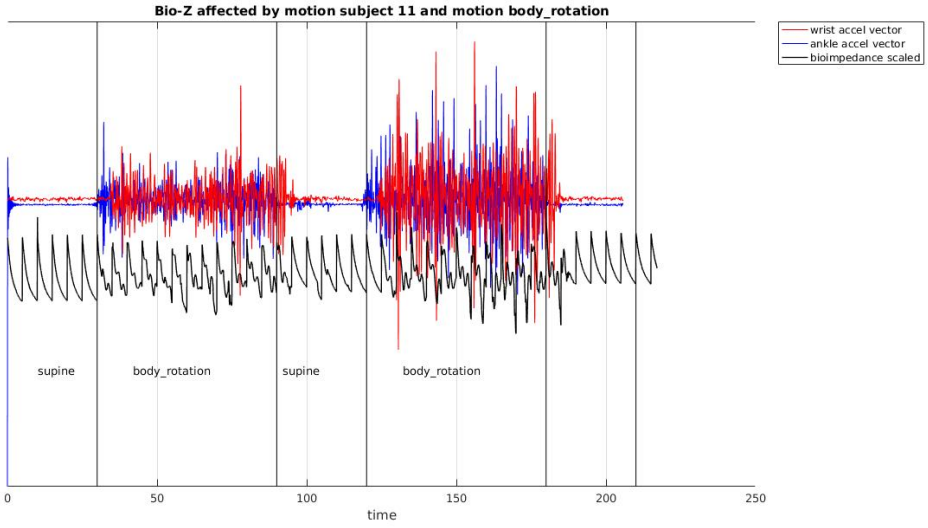

(b) Bioimpedance signal affected due to the rotation of the body

Figure 4.9: Plots illustrating variation in bioimpedance signal due to motion. The z axis of the wrist accelerometer is shown in this illustration.

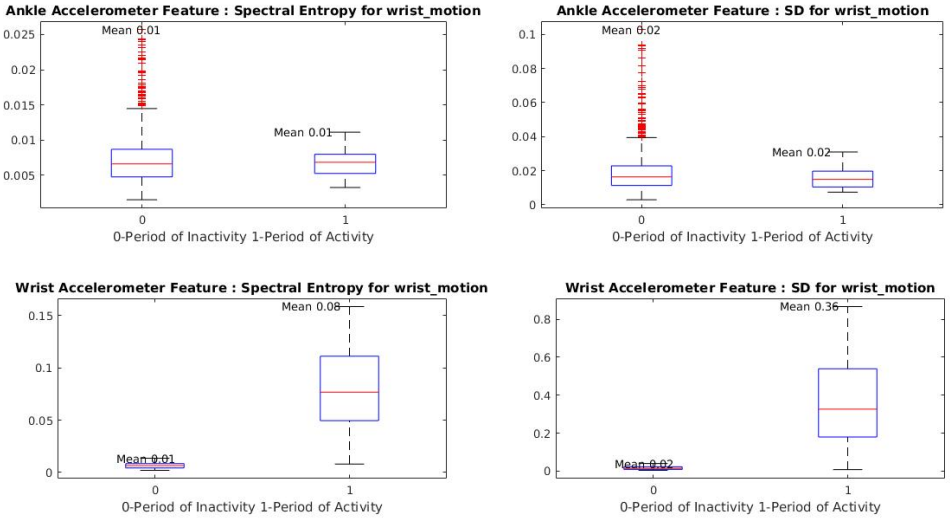

(a) Magnitude of features extracted during Wrist Rotation

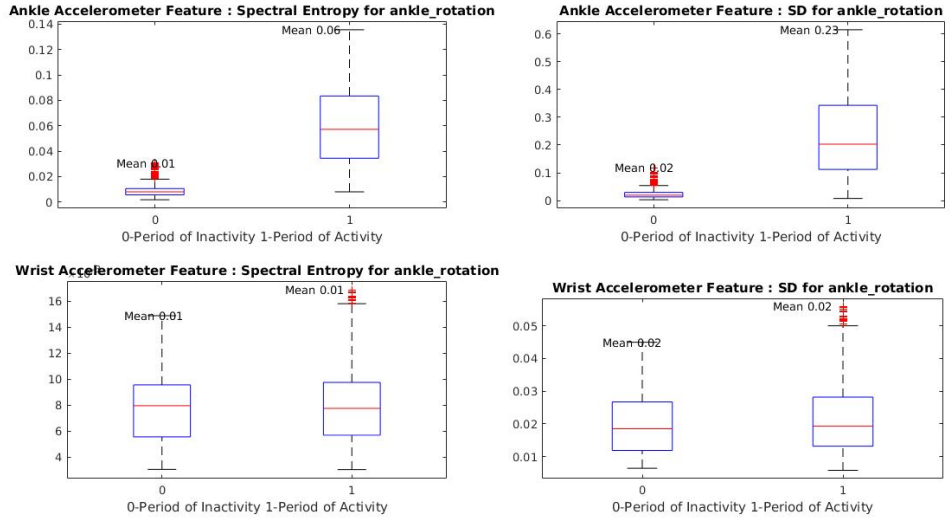

(b) Magnitude of features extracted during Ankle Rotation

Figure 4.10: Box plots showing the magnitude of feature extracted for wrist and ankle rotation. Note : for this figure y axis is in the scale of 10^{-3}. Also refer Appendix A.3.2.

The 10 fold cross validated approach was proposed in section 3.3.2 and tested with a decision tree and svm model for classifications. The decision tree and svm model proposed in this work had comparable misclassification loss. The average loss for the models are presented in Appendix A.3. The third fold of the decision tree had the lowest loss (0.0191) and this was less than the lowest loss observed for the svm model (0.021). The model evaluation metrics on the training and testing data sets are presented in Table 4.5. The ROC curves for the model and area under curve(AUC) is presented in Figure 4.11. AUC > 0.9 for both models indicates that the classifier is able to identify the periods movement at a satisfactory level.

	Decision Tree		SVM	
	Training Set	Testing Set	Training Set	Testing Set
Accuracy	97.63 ± 0.015	97.51 ± 0.013	97.25 ± 0.014	97.47 ± 0.013
Sensitivity	97.92	98.28	98.31	98.32
Specificity	97.07	95.35	95.2	95.14

Table 4.5: Model evaluation Metrics (in %) for Movement Identification. Accuracy presented as mean $\pm$ standard deviation

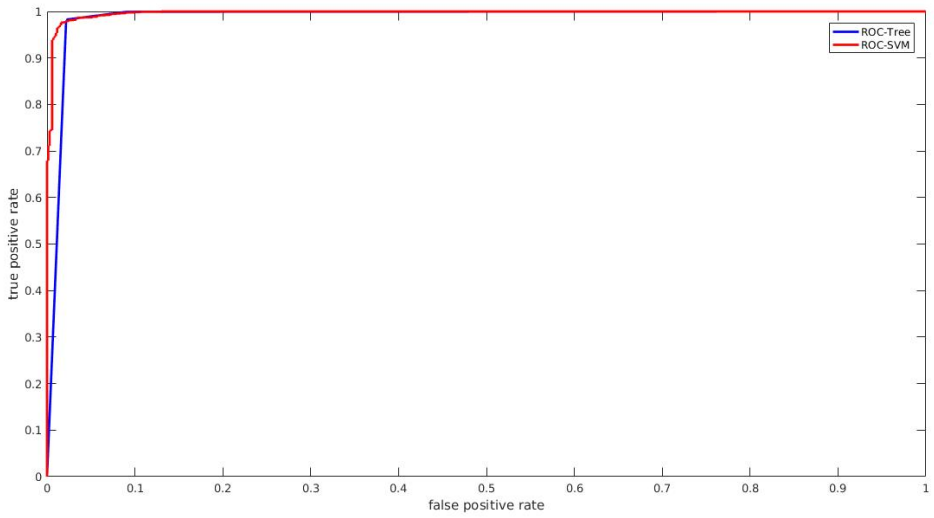

Figure 4.11: ROC curves for both models show high true positive rates and low false positive rates.AUC for svm = 0.997 , AUC for decision tree = 0.988

Figure 4.12 illustrates the usage of the framework presented to classify periods of activity and inactivity.

The achieved accuracy levels were comparable to levels found in literature [44] & [47]. At these accuracy levels consistent information regarding movement during bioimpedance measurements can be retrieved. Although a few misclassifications are encountered, the incidence is at random one-off instances which do not reduce the performance of the approach.

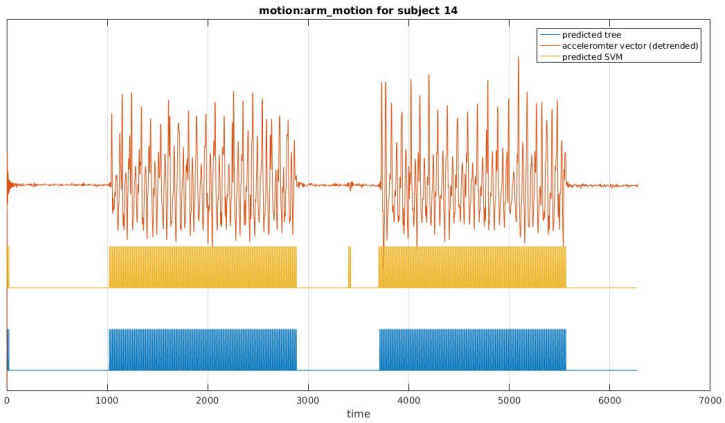

(a)

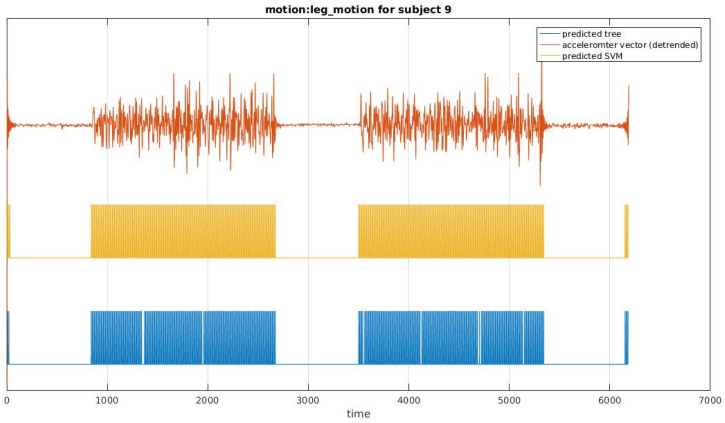

(b)

Figure 4.12: Illustration of generating movement context
The high states of the prediction indicate presence of motion /activity and vice versa.
(legend ref :yellow : predicted state from SVM.blue : predicted state from tree.red:de-trended accelerometer signal. Hi - Level : Active Period. Lo - Level : Inactive Periods)

4.4.2 Body Posture Detection

The work undertaken in this thesis is to identify gross body postures like supine posture, sitting and standing.

The thigh and ankle accelerometer pair are used to identify the angles associated with the body postures.

Theoretically from the experimental design and setup, the **ideal** results would correspond to

- When the person is in supine position the cosine angle of the z axis vector is zero degrees for both thigh and ankle accelerometers.
- When the person is sitting , the cosine angle of the z axis vector is zero degrees for the thigh and ninety degrees for the ankle accelerometer.
- Similarly, when the person is standing the angle of the z axis vector is ninety degrees for both ankle and thigh accelerometers.

The experimental sequence of posture changes with the corresponding accelerometer angles calculated is illustrated in Figure 4.13.

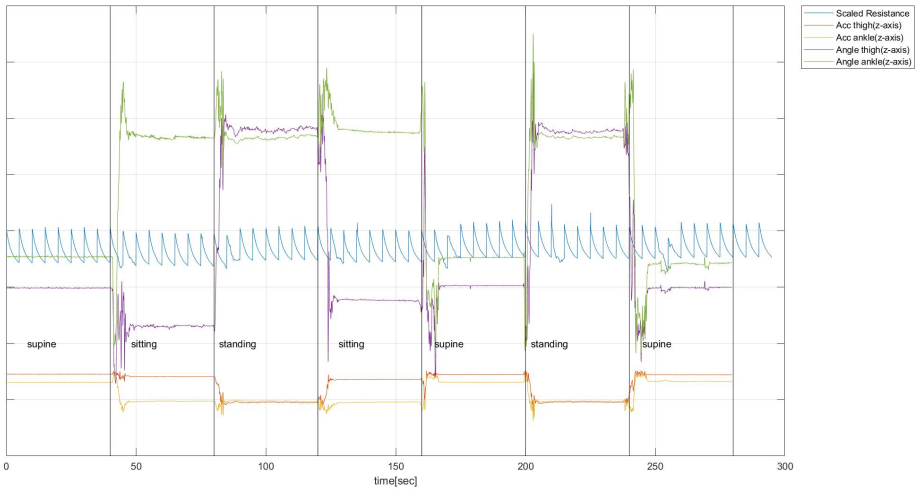

Figure 4.13: Illustration of the experimental sequence with the corresponding angles measured Yellow and orange lines denote the z axis of the accelerometers. The green and purple lines denote the angles calculated from the ankle and thigh accelerometer respectively.

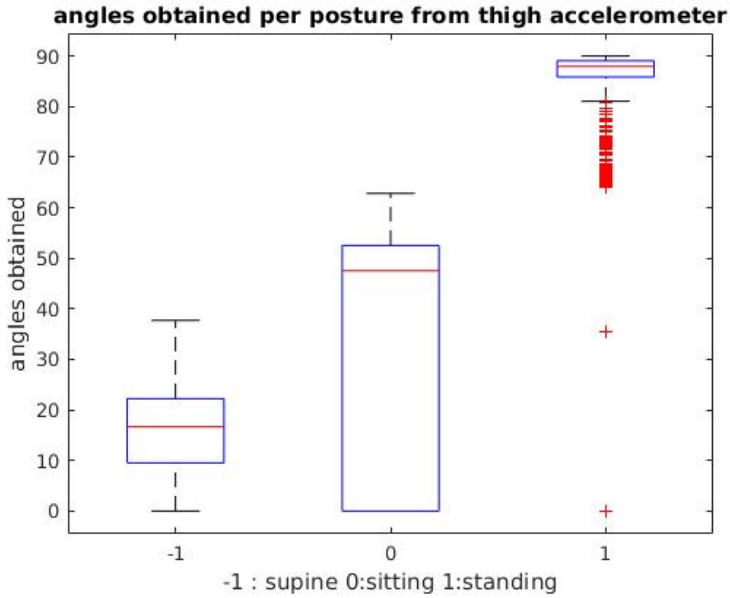

(a) Thigh accelerometer range of angles for each posture for all subjects

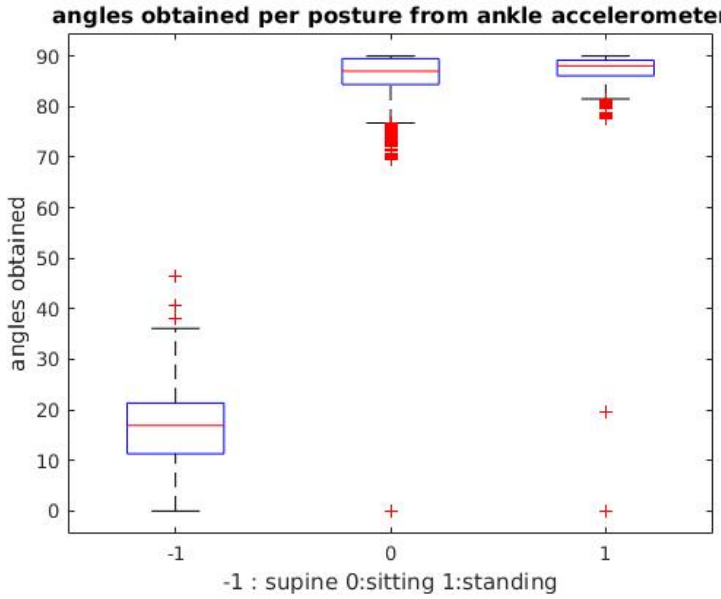

(b) Ankle accelerometer range of angles for each posture for all subjects

Figure 4.14: Angles measured in **degrees** for each position using ankle and thigh accelerometer

Table 4.6 below presents the mean, median and standard deviation for the angles measured.

	Ankle Accelerometer			Thigh Accelerometer		
	Supine	Sitting	Standing	Supine	Sitting	Standing
Mean ± SD	15.72±8.74	75.82±28.95	88.01±17.93	15.46±10.01	32.80±24.61	71.86±34.09
Median	16.95	86.99	88.023	16.68	47.45	87.92

Table 4.6: Mean , Standard Deviation and Median values of angles measured in degrees for all subjects.

The test set accuracy on the posture detection was 94.6%. The sensitivity for supine, sitting and standing postures were 96.1% ,92.8% and 94.1% respectively. The specificity for supine, sitting and standing postures were 96.1%, 97.3% and 98.3% respectively. The precision scored were 94.8%, 93.3% and 95.6% respectively.

For the detection of transitions, the contexts generated from the previous section and the angles measured from this section help to identify the transitions. During a transition period a short interval of high states is indicated by the output stage of the previously discussed models and post that short burst, the output is stabilized to a low state classification with the acquired angles from the present model. An illustration of this is seen in Figure 4.15.

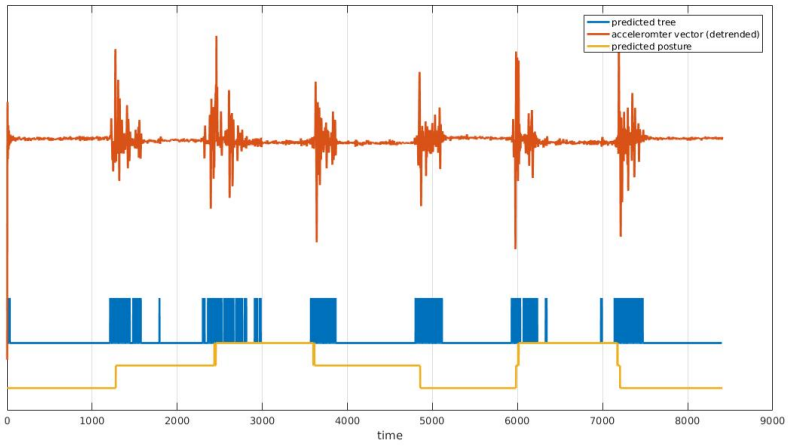

Figure 4.15: Illustration of detection of transition and postures
The posture estimated is represented by the yellow line. (-1 level:Supine , 0 level:Sitting and 1 level:Standing). The blue line represents the motion detected. It is visually apparent that during transitions the motion contexts are generated at the same time that a transition in posture is seen. This is before the motion signal stabilizes into an inactive period post the posture change.

4.4.3 Discussion

The results presented in the previous section indicate that the work undertaken in this thesis could recognize two significant contexts with sufficient accuracy (>95%). Firstly, periods of activity(dynamic) and periods of inactivity(static) were recognized using the accelerometer signals from the wrist and ankle. Secondly, the gross postures of the subjects were identified using the accelerometer signals from the thigh and the ankle.

Activity Classification

From Figure 4.10 we see that for upper body related motion the wrist accelerometer provides a satisfactory level of motion estimate and for lower body related motion the ankle accelerometer provides a satisfactory level of motion estimate. From Figure 4.10(a) it is noticeable that for wrist motion, only the wrist accelerometer shows a difference in the feature extracted during periods of motion and non motion. Similar observations can be made for other plots as well. Leg rotation was the best distinguished motion with a greatly demarcated mean between the two periods. It was also observed that the magnitude of the standard deviation feature extracted during periods of motion was greater than the magnitude of the spectral entropy feature during the same periods. This would indicate that the standard deviation has more predictive power. Going forward it would be prudent to consider only this feature for classification provided that there is no drop in the levels of performance. Using standard deviation as a feature will also reduce the computational needs of the system as compared to performing fourier transform for spectral entropy.

Results in [45] incorporates mean and standard deviation with a SVM classifier to perform activity classification at an accuracy of 97.4%. A similar accuracy was also observed by [46] incorporating signal magnitude and neural classifiers. Results by [48] reported an accuracy of 92% when spectral entropy was incorporated in decision tree topology. In comparison with these results the classification approach undertaken in this work is comparable in performance to the results seen previously.

Posture Classification

Figure 4.14 illustrates the measured angles for each position with the thigh and ankle accelerometer. From the figure it is seen that unlike the ideal case, a range of values is measured that is in close agreement with the ideal scenario. For the thigh accelerometer, the range of angles for the sitting position is large because of the fact that not all subjects tend to sit with the femur and shin at perfect ninety degree angles. The figures also indicate that the angles measured using the thigh accelerometer is crucial for differentiating supine and sitting position from standing position, while the ankle accelerometer is crucial for differentiating between standing and sitting from the supine position. This observation is a justification for the use of ankle-thigh accelerometers for posture detection.

Contextual Monitoring

Section 2.3.1 & 2.3.2 has emphasized the requirement of movement related data (that represents motion artifacts and posture) in context with bioimpedance signals. Therefore, consistent information regarding motion during bioimpedance measurements is required to compensate motion artifacts and posture related signal variability.

Whole body bioimpedance measurements consistently show changes in the measured values with varying postures. Generating postural contexts enables the system to accommodate variations seen in the bioimpedance with changing position. This would help make informed clinical interpretations of the data recorded by clearly marking a variation (increase or decrease) in the measured impedance values with the specific postural context. Going further, investigations related to the utilization of mathematical modeling of postural factors and their influence on the measurements will improve the accuracy of bioimpedance spectroscopy for continuous monitoring.

Determination of static and dynamic activity contexts during measurements provides a couple of advantages. The approach firstly provides the opportunity to obtain high quality and reliable impedance measurements by logging measurements only during static activity periods. Secondly, the prediction of the context can be utilized to automatically classify the measured data into two segments. The bioimpedance measurement in the first segment represents the data measured when there is no motion. This set of measurements will be of high quality (considering there are no faults in the other parts of the system) and unaffected by motion artifacts. The data in the second segment is affected by motion artifacts and hence contains a noisy signal. The treatment of data in this segment is dependent on what is required clinically. In the study [45], the data within this segment was discarded as it wasn't clinically important. In this specific scenario, to identify prognostic events for dengue fever, continuous measurements lasting 48 hours is required.

The time duration between the occurrence of the shock episode and clinical management protocol (fluid administration) is quite small and the progression of the condition is fast. Therefore, every window of signal acquired is important. With these requirements, it is firstly desirable to identify those instances when the quality of signal was affected due to the patient's motion and more importantly retrieve the noisy data in the segment and reconstruct the signal to obtain valid data.

The ability of the system to perform these tasks will translate the technology towards unsupervised systems without the requirement of special measurement settings.

Limitations

- Time Stamps & Labels : In this work the time stamps were maintained in an inefficient manner through timers. As a result while segregating the data, outliers were encountered at the transitions. In future experiments using video or feedback (push buttons) references will help generate better time stamps.

- The experimental study for generating motion artifacts was ideal in this study. Going forward a combination of motions (for instance movement of wrist and ankle)which is likely to be encountered in everyday situations must be considered. This would not affect the way the classification or motion identification approach behaves. This will help improve the framework proposed for future development stages (reconstruction of signal).

- The accelerometers in this work have been configured to poll data the entire time. However, it would be more beneficial if the accelerometers are configured through interrupts to decrease the power consumption.

- The measurements and recordings were not performed on dengue affected subjects. The movements and the sequence of movements were controlled. In the future, long term recordings on dengue affected subjects without any specific movement task should be performed.

Chapter 5

Conclusion

A motion aware bioimpedance measurement system (AMBICA) was presented in this work to address key engineering gaps for continuous fluid monitoring in dengue patients. The performance of AMBICA was compared to the commercial BIACorpus system. AMBICA has indicated the capability to measure whole body bio-impedance values within the same range as BIACorpus. The results indicate the presence of a systematic error for both impedance and reactance measurements. The bias was lower for impedance measurements (bias = - 4.50) as compared to reactance measurements(bias = 14.84). In addition precision scores from Figure 4.8 indicated that the repeatability of AMBICA was superior to BIACorpus. The agreement between the devices was close only for impedance measurements and a lack of agreement was observed for reactance measurements. Due to inconsistencies and errors observed with both the devices, (during reactance measurements) it is challenging to assess the true performance of AMBICA. While on one hand AMBICA has showed promising results with impedance measurements, the reactance measurements are in disagreement. However, from Figure 4.2, we see that the reactance measurements of AMBICA acquired here are in closer agreement both to observations in literature and to physiological occurrences. Therefore, AMBICA has shown promise from the healthy volunteer study and can subsequently be used for further clinical experiments with two important considerations. First, a prior acceptable limit of error must be decided upon with the feedback from clinical researchers. Second, continuous observations related to the behavior of R-Xc curve after the characteristic frequency must be made. If the results obtained are similar to that of the inconsistencies observed in this study then modifications to the recording system is required. In addition to the the earlier analysis, this work also proposed a framework to gather vital motion related information like the position and periods of activity. The classification task undertaken was promising. This framework can be potentially adapted into developing contextual bioimpedance monitoring applications to better understand the effects of posture and motion on the bioimpedance signal.

In the future AMBICA will benefit from translating the current prototype device into an integrated version in a wearable form. The device needs to be light, low in power consumption, high computational power and a good user interface. This will improve the usability of the device for both the patients and the clinicians. The wearable system powered by the contextual monitoring algorithm has the potential to bridge techno-clinical gaps and tailor a smart bioimpedance measurement system.

Bibliography

[1] Bhatt S, Gething PW, Brady OJ, Messina JP, Farlow AW, Moyes CL et.al. The global distribution and burden of dengue. Nature;496:504-507.

[2] Kularatne, S.A., Weerakoon, K.G., Munasinghe, R. et al. Trends of fluid requirement in dengue fever and dengue haemorrhagic fever: a single centre experience in Sri Lanka. BMC Res Notes 8, 130 (2015) doi:10.1186/s13104-015-1085-0

[3] Ibrahim, Fatimah, et al. "A novel approach to classify risk in dengue hemorrhagic fever (DHF) using bioelectrical impedance analysis (BIA)." IEEE transactions on instrumentation and measurement 54.1 (2005): 237-244.

[4] Gonzalez, C. H., et al. "Total body water measurement using bioelectrical impedance analysis, isotope dilution and total body potassium: a scoring system to facilitate intercomparison." European journal of clinical nutrition 56.4 (2002): 326.

[5] S. Grimnes and Ø. Martinsen, Bioimpedance and Bioelectricity Basics , Academic Press, London, UK, 3rd edition, 2014

[6] L. M. Roa, D. Naranjo, J. Reina-Tosina et al., "Applications of bioimpedance to end stage renal disease (ESRD)," Studies in Computational Intelligence ,vol.404,pp.689–769,2013.

[7] https://www.getbodysmart.com/nervous-system/ion-channel-proteins

[8] Kyle, Ursula G., et al. "Bioelectrical impedance analysis—part I: review of principles and methods." Clinical nutrition 23.5 (2004): 1226-1243.

[9] Brantlov, Steven, et al. "Critical factors and their impact on bioelectrical impedance analysis in children: a review." Journal of medical engineering & technology 41.1 (2017): 22-35.

[10] Naranjo-Hernández, David, Javier Reina-Tosina, and Mart Min. "Fundamentals, recent advances, and future challenges in bioimpedance devices for healthcare applications." Journal of Sensors 2019 (2019).

[11] Jaffrin, Michel Y., and Hélène Morel. "Body fluid volumes measurements by impedance: A review of bioimpedance spectroscopy (BIS) and bioimpedance analysis (BIA) methods." Medical engineering & physics 30.10 (2008): 1257-1269.

[12] Ulbrich, Mark, et al. ”Analysis of Body Segments using Bioimpedance Spectroscopy and Finite Element Method

[13] Luna, José Luis Vargas, et al. ”Dynamic impedance model of the skin-electrode interface for transcutaneous electrical stimulation.” PloS one 10.5 (2015): e0125609.

[14] Buxi, Dilpreet, et al. ”Correlation between electrode-tissue impedance and motion artifact in biopotential recordings.” IEEE sensors journal 12.12 (2012): 3373-3383.

[15] de Talhouet, Hughes, and John G. Webster. ”The origin of skin-stretch-caused motion artifacts under electrodes.” Physiological Measurement 17.2 (1996): 81.

[16] Cömert, Alper, and Jari Hyttinen. ”Investigating the possible effect of electrode support structure on motion artifact in wearable bioelectric signal monitoring.” Biomedical engineering online 14.1 (2015): 44.

[17] Stanslaski, Scott, et al. ”Design and validation of a fully implantable, chronic, closed-loop neuromodulation device with concurrent sensing and stimulation.” IEEE Transactions on Neural Systems and Rehabilitation Engineering 20.4 (2012): 410-421.

[18] Virtanen, Jaakko, et al. ”Accelerometer-based method for correcting signal baseline changes caused by motion artifacts in medical near-infrared spectroscopy.” Journal of biomedical optics 16.8 (2011): 087005.

[19] Sweeney, Kevin T., Tomás E. Ward, and Seán F. McLoone. ”Artifact removal in physiological signals—Practices and possibilities.” IEEE transactions on information technology in biomedicine 16.3 (2012): 488-500.

[20] Medrano, Guillermo, Steffen Leonhardt, and Peng Zhang. ”Modeling the influence of body position in bioimpedance measurements.” 2007 29th Annual International Conference of the IEEE Engineering in Medicine and Biology Society. IEEE, 2007.

[21] Rush, Elaine C., et al. ”Validity of hand-to-foot measurement of bioimpedance: standing compared with lying position.” Obesity 14.2 (2006): 252-257.

[22] Sahakian, Alan V., Willis J. Tompkins, and John G. Webster. ”Electrode motion artifacts in electrical impedance pneumography.” IEEE transactions on biomedical engineering 6 (1985): 448-451.

[23] Khambete, N. D., B. H. Brown, and R. H. Smallwood. ”Movement artefact rejection in impedance pneumography using six strategically placed electrodes.” Physiological measurement 21.1 (2000): 79.

[24] Boone, K. G., and D. S. Holder. ”Current approaches to analogue instrumentation design in electrical impedance tomography.” Physiological measurement 17.4 (1996): 229.

[25] Petrova, Galidia I. "Influence of electrode impedance changes on the common-mode rejection ratio in bioimpedance measurements." Physiological measurement 20.4 (1999): N11.

[26] Chaloemwong, Juthatip, et al. "Useful clinical features and hematological parameters for the diagnosis of dengue infection in patients with acute febrile illness: a retrospective study." BMC hematology 18.1 (2018): 20.

[27] https://www.maximintegrated.com/en/design/technical-documents/tutorials/1/1080.html

[28] Ross, Alexander S., et al. "Current source design for electrical impedance tomography." Physiological measurement 24.2 (2003): 509.

[29] Implementing the AD5940 and AD8233 in a Full Bioelectric System - Application Note AN-1557

[30] Vela, Luis M., et al. "Standalone IoT Bioimpedance Device Supporting Real-Time Online Data Access." IEEE Internet of Things Journal 6.6 (2019): 9545-9554.

[31] Ferreira, Javier, et al. "AD5933-based spectrometer for electrical bioimpedance applications." Journal of Physics: Conference Series. Vol. 224. No. 1. IOP Publishing, 2010.

[32] Dittmar, Manuela, and Helmut Reber. "Validation of different bioimpedance analyzers for predicting cell mass against whole-body counting of potassium (40K) as a reference method." American Journal of Human Biology: The Official Journal of the Human Biology Association 16.6 (2004): 697-703.

[33] Genton, Laurence, et al. "Bioimpedance-derived phase angle and mortality among older people." Rejuvenation research 20.2 (2017): 118-124.

[34] Tanabe, Roberta Falcão, et al. "Distribution of bioelectrical impedance vector values in multiethnic infants and pre-school children." Clinical Nutrition 31.1 (2012): 144-148.

[35] Silva, Analiza M., et al. "Lack of agreement of in vivo raw bioimpedance measurements obtained from two single and multi-frequency bioelectrical impedance devices." European journal of clinical nutrition 73.7 (2019): 1077-1083.

[36] Naranjo-Hernández, David, et al. "Smart Bioimpedance Spectroscopy Device for Body Composition Estimation." Sensors 20.1 (2020): 70.

[37] Thomas, B. J., B. H. Cornish, and L. C. Ward. "Bioelectrical impedance analysis for measurement of body fluid volumes: a review." Journal of clinical engineering 17.6 (1992): 505-510.

[38] MON-PO490: Bioelectrical Impedance Analysis Devices: Are Their Raw Measurements Interchangeable? Gonzalez, M.-C. Clinical Nutrition, Volume 38, S239 - S240

[39] Ward LC, Byrne NM, Rutter K, Hennoste L, Hills AP, Cornish BH, et al. Reliability of multiple frequency bioelectrical impedance analysis: an intermachine comparison. Am J Human Biol:Off J Human Biol Counc. 1997;9:63–72.

[40] Kassanos, Panagiotis, et al. "An integrated analog readout for multi-frequency bioimpedance measurements." IEEE Sensors Journal 14.8 (2014): 2792-2800.

[41] Hersek, Sinan, et al. "Wearable vector electrical bioimpedance system to assess knee joint health." IEEE Transactions on Biomedical Engineering 64.10 (2016): 2353-2360.

[42] Sanchez, Benjamin, et al. "Novel estimation of the electrical bioimpedance using the local polynomial method. Application to in vivo real-time myocardium tissue impedance characterization during the cardiac cycle." IEEE Transactions on Biomedical Engineering 58.12 (2011): 3376-3385.

[43] Preece, Stephen J., et al. "Activity identification using body-mounted sensors—a review of classification techniques." Physiological measurement 30.4 (2009): R1.

[44] Hersek, Sinan, Hakan Töreyin, and Omer T. Inan. "A robust system for longitudinal knee joint edema and blood flow assessment based on vector bioimpedance measurements." IEEE transactions on biomedical circuits and systems 10.3 (2015): 545-555.

[45] Hersek, Sinan, et al. "Wearable vector electrical bioimpedance system to assess knee joint health." IEEE Transactions on Biomedical Engineering 64.10 (2016): 2353-2360.

[46] Farkas, Ioana, and Elena Doran. "Activity recognition from acceleration data collected with a tri-axial accelerometer." Acta Technica Napocensis 52.2 (2011): 38.

[47] Lugade, Vipul, et al. "Validity of using tri-axial accelerometers to measure human movement—Part I: Posture and movement detection." Medical engineering & physics 36.2 (2014): 169-176.

[48] Celka, P., et al. "Motion resistant earphone located infrared based heart rate measurement device." Biomedical Engineering (2004).

[49] He, Zhenyu. "Activity recognition from accelerometer signals based on wavelet-ar model." 2010 IEEE International Conference on Progress in Informatics and Computing. Vol. 1. IEEE, 2010.

[50] Anania, Gaetano, et al. "Development of a novel algorithm for human fall detection using wearable sensors." SENSORS, 2008 IEEE. IEEE, 2008.

[51] Wu, Winston H., et al. "Context-aware sensing of physiological signals." 2007 29th Annual International Conference of the IEEE Engineering in Medicine and Biology Society. IEEE, 2007.

[52] Hostettler, Roland, et al. "Motion Artifact Reduction in Ambulatory Electrocardiography Using Inertial Measurement Units and Kalman Filtering." 2018 21st International Conference on Information Fusion (FUSION). IEEE, 2018.

[53] Kunnath, Abishek Thekkeyil, et al. ”wicard: A context aware wearable wireless sensor for cardiac monitoring.” 2013 International Conference on Advances in Computing, Communications and Informatics (ICACCI). IEEE, 2013.

[54] Cecconi, Maurizio, et al. ”Bench-to-bedside review: the importance of the precision of the reference technique in method comparison studies–with specific reference to the measurement of cardiac output.” Critical care 13.1 (2009): 201.

[55] Ward, Leigh C., and Bruce H. Cornish. ”Bioelectrical impedance analysis at the characteristic frequency.” Nutrition 23.1 (2007): 96.

[56] Ayllón, David, Roberto Gil-Pita, and Fernando Seoane. ”Detection and classification of measurement errors in bioimpedance spectroscopy.” PloS one 11.6 (2016): e0156522.

[57] Naranjo-Hernández, David, Javier Reina-Tosina, and Mart Min. ”Fundamentals, recent advances, and future challenges in bioimpedance devices for healthcare applications.” Journal of Sensors 2019 (2019).

Appendix A

Appendix

A.1 Scatter Plots

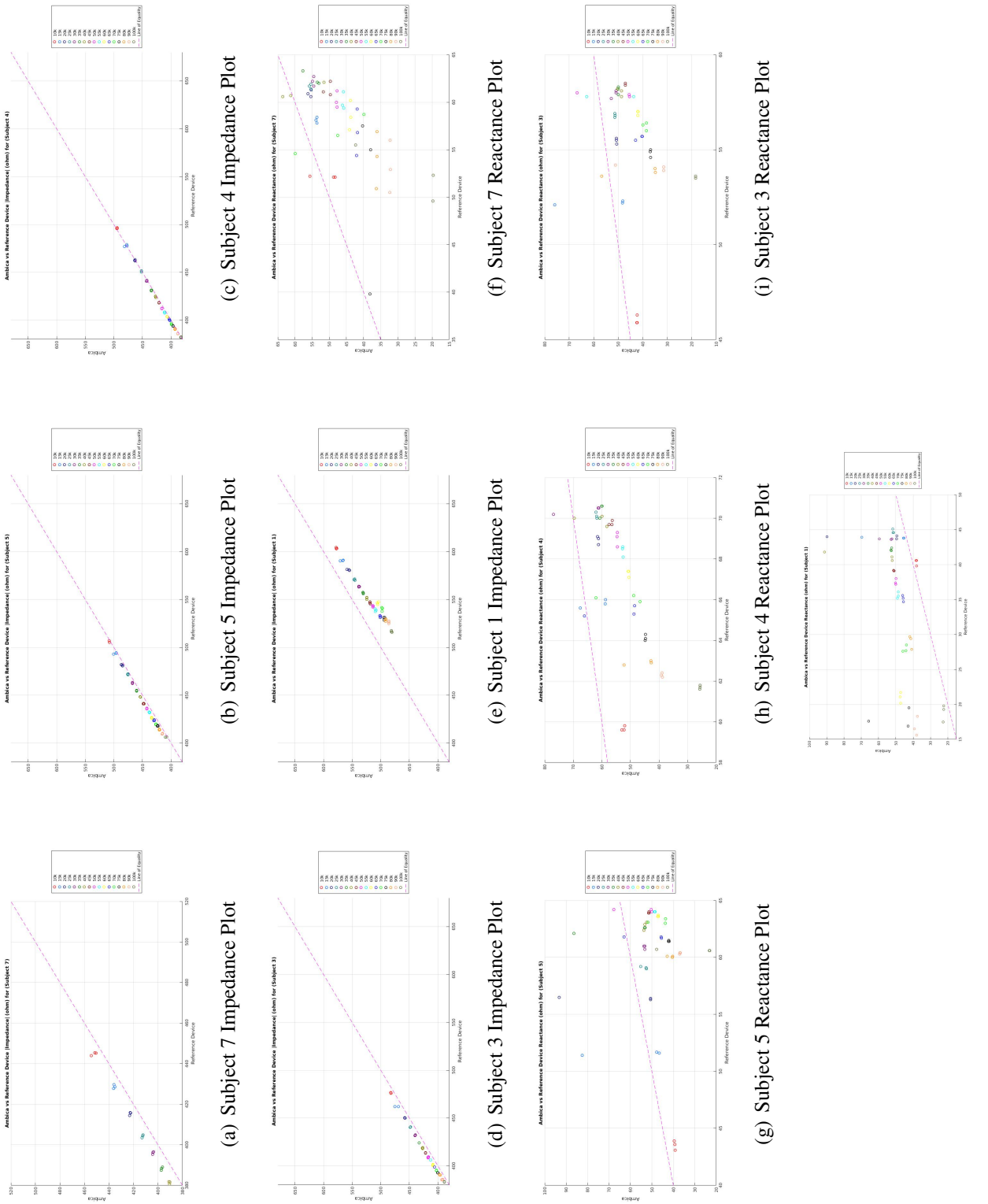

(a) Subject 7 Impedance Plot (b) Subject 5 Impedance Plot (c) Subject 4 Impedance Plot

(d) Subject 3 Impedance Plot (e) Subject 1 Impedance Plot (f) Subject 7 Reactance Plot

(g) Subject 5 Reactance Plot (h) Subject 4 Reactance Plot (i) Subject 3 Reactance Plot

(j) Subject 1 Reactance Plot

Figure A.1: AMBICA vs BIACorpus plots for impedance and reactance.Data Points at each frequency is color coded.

A.2 Impedance measurement BA plots for every subject

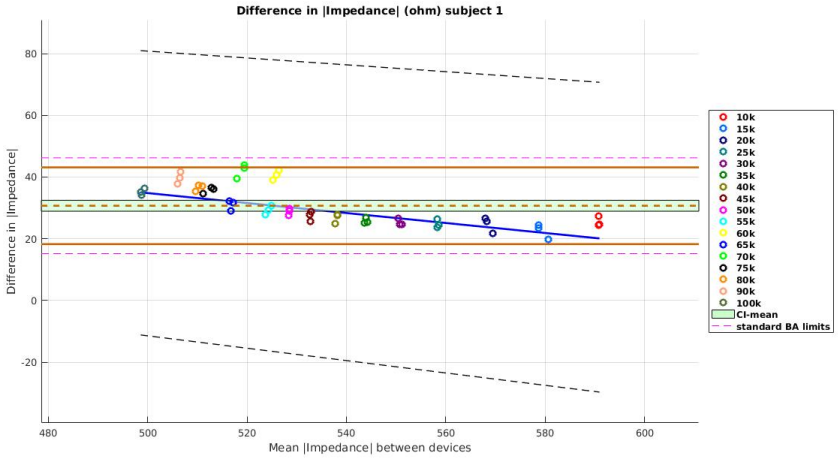

(a) Subject 1 Impedance Plot.The dotted black line for shows the updated CI using regression to accommodate the highly significant trend seen in BA plot

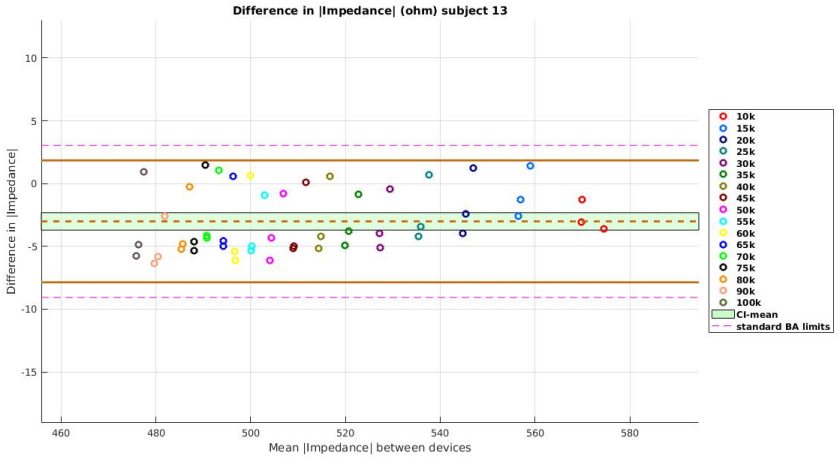

(b) Subject 13 Impedance Plot

Figure A.2: Bland Altman Plots for Impedance Measurements - 1
The dotted line in pink is denotes the 95% confidence interval limits for limits of agreement (LoA) calculated with standard bland altman equations.The solid line in orange represents the LoA.The bias is represented by the thick dotted line in orange

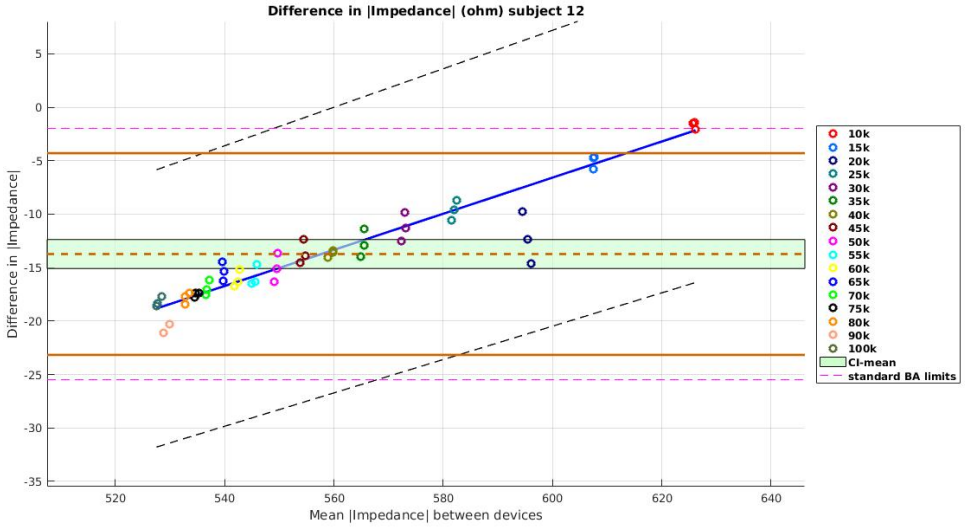

(a) Subject 12 Impedance Plot.The dotted black line for shows the updated CI using regression to accommodate the highly significant trend seen in BA plot

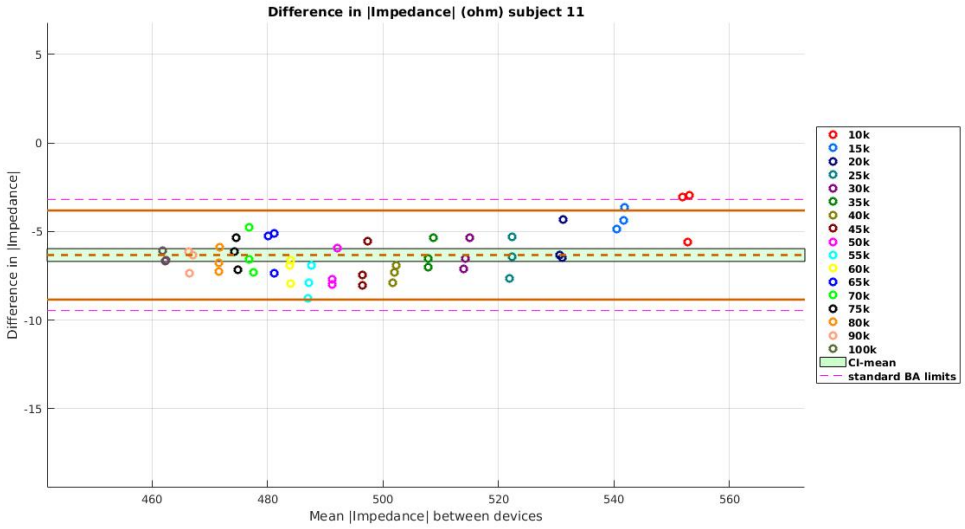

(b) Subject 11 Impedance Plot

Figure A.3: Bland Altman Plots for Impedance Measurements - 2

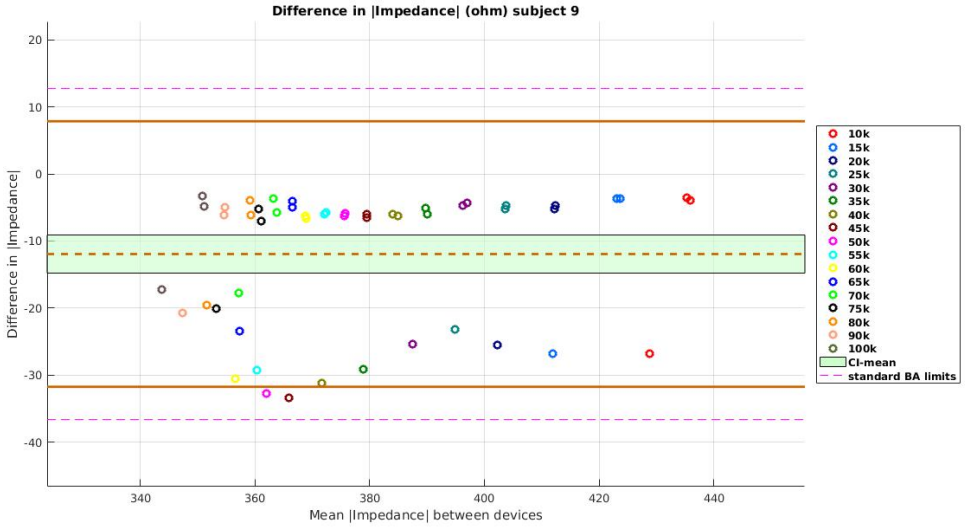

(a) Subject 9 Impedance Plot

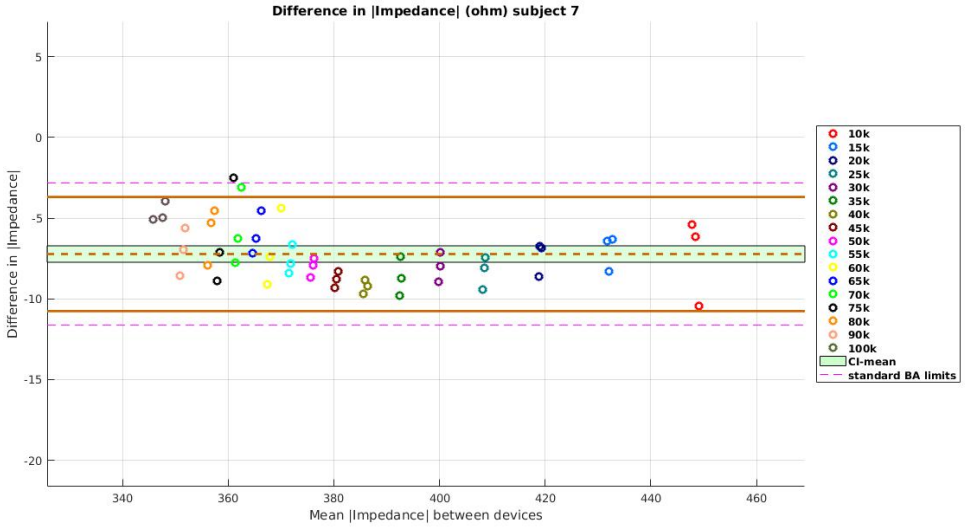

(b) Subject 7 Impedance Plot

Figure A.4: Bland Altman Plots for Impedance Measurements - 3

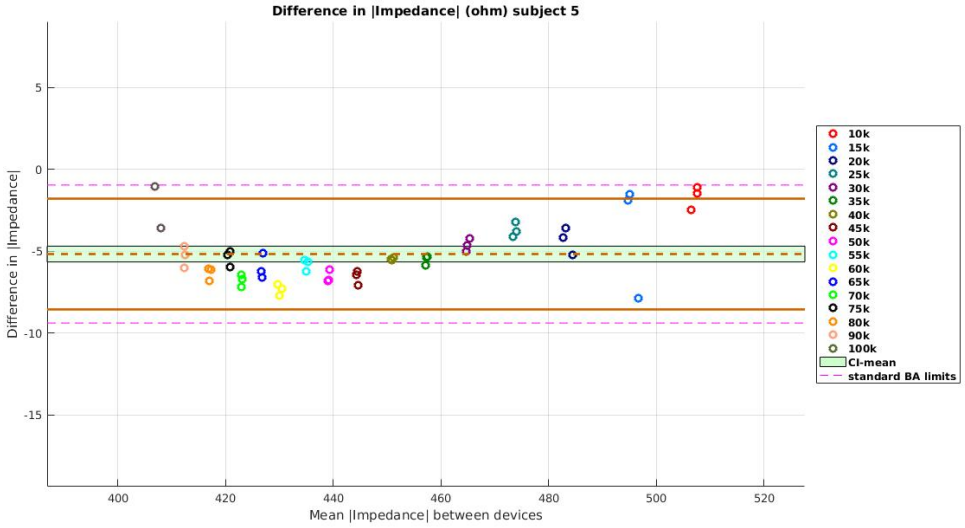

(a) Subject 5 Impedance Plot

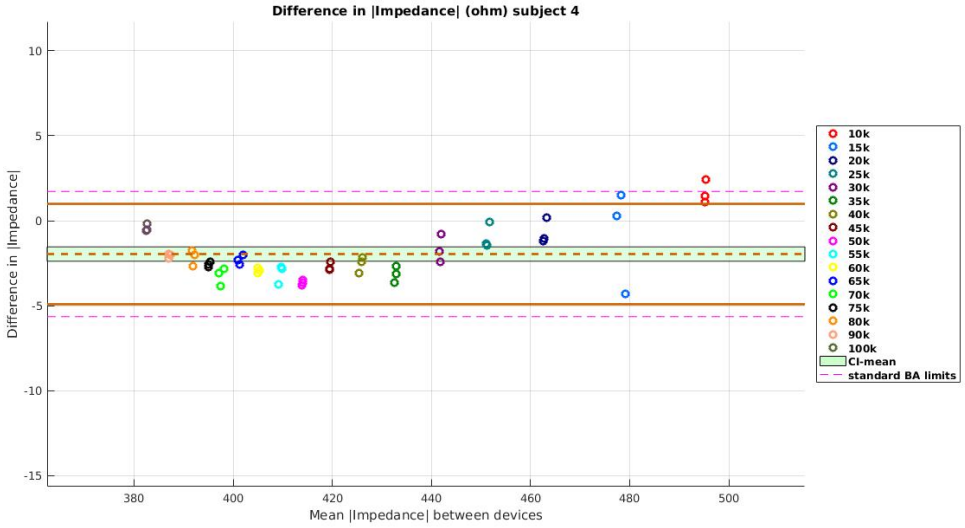

(b) Subject 4 Impedance Plot

Figure A.5: Bland Altman Plots for Impedance Measurements - 4

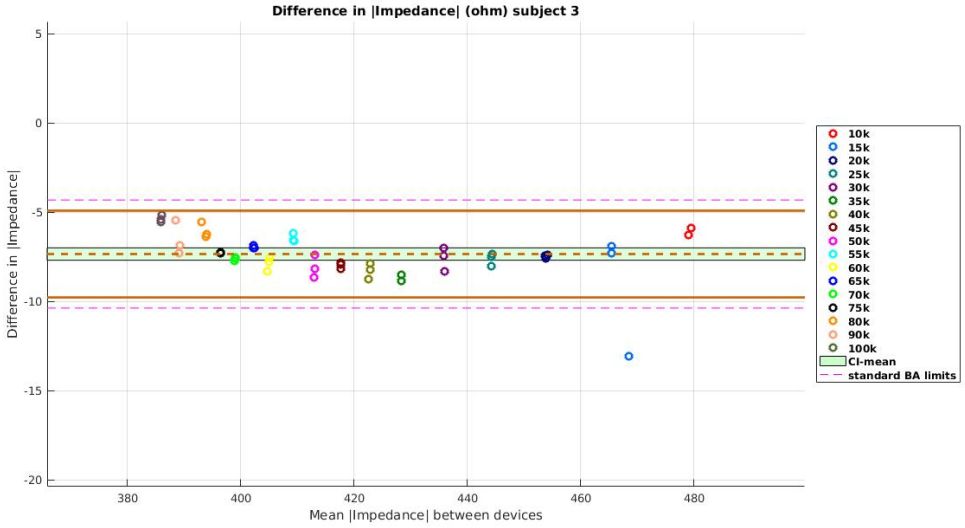

(a) Subject 3 Impedance Plot

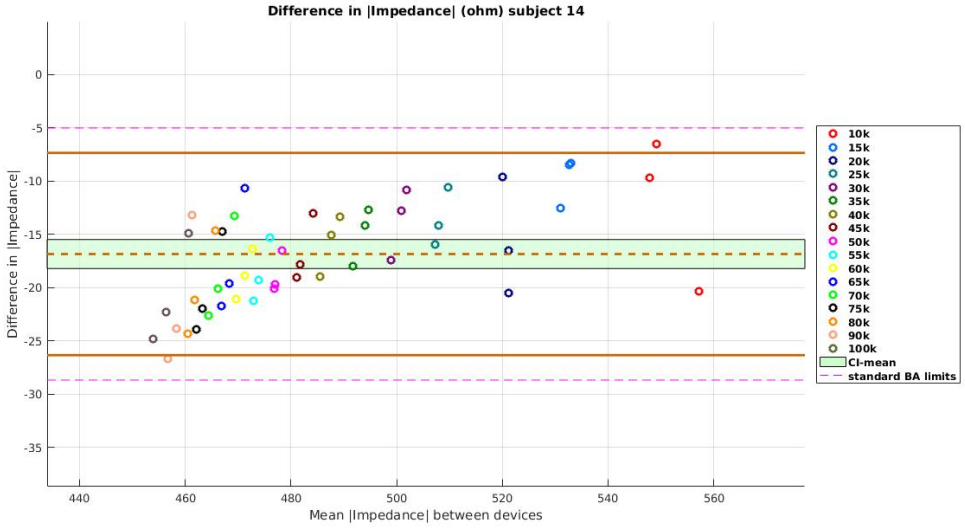

(b) Subject 14 Impedance Plot

Figure A.6: Bland Altman Plots for Impedance Measurements - 5

A.3 Reactance measurement BA plots for every subject

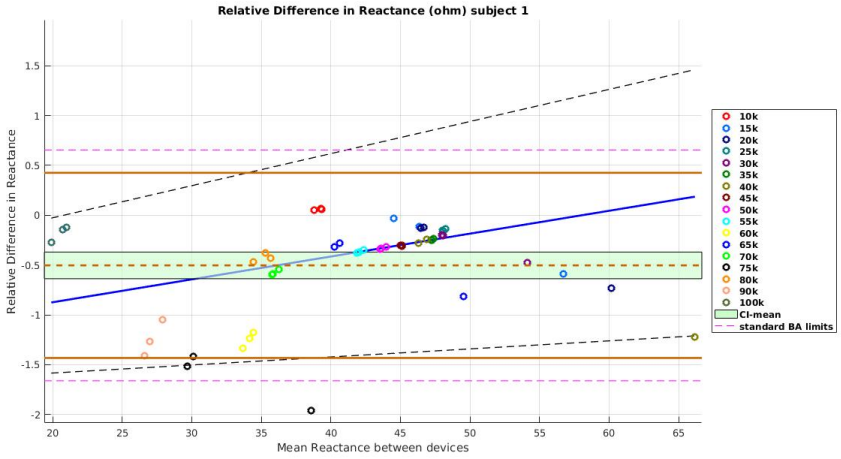

(a) Subject 1 Reactance Plot

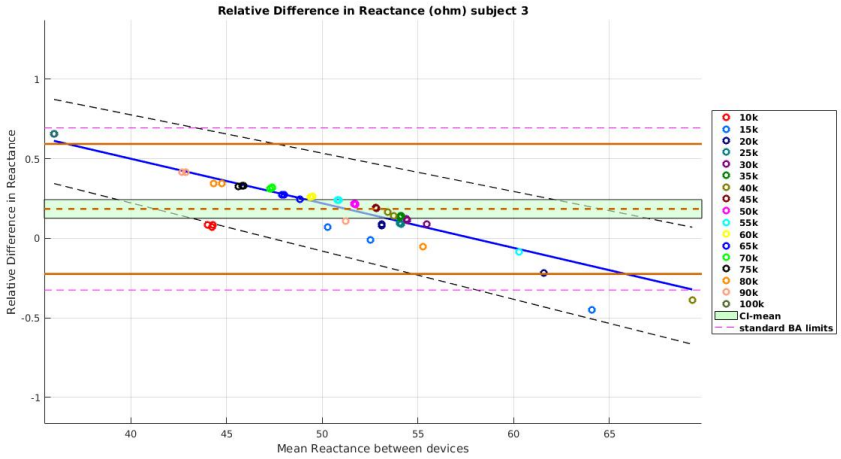

(b) Subject 3 Reactance Plot

Figure A.7: Bland Altman Plots for Reactance Measurements - 1
Note: y-axis is relative difference (Reference - AMBICA) / Reference.

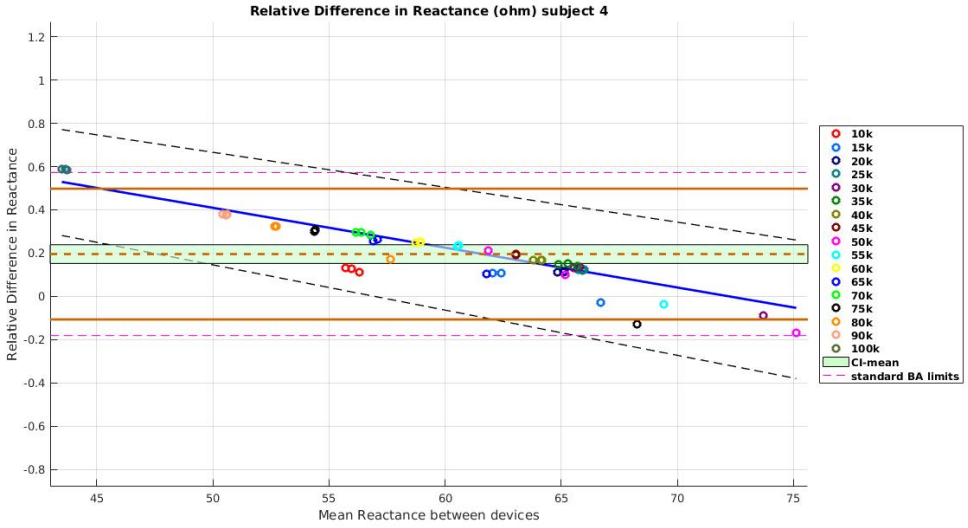

(a) Subject 4 Reactance Plot

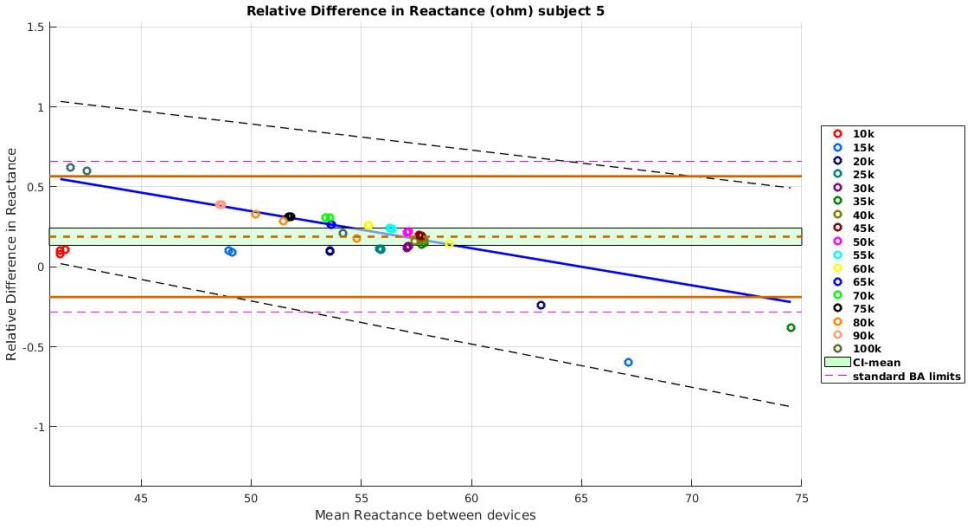

(b) Subject 5 Reactance Plot

Figure A.8: Bland Altman Plots for Reactance Measurements - 2
Note: y-axis is relative difference (Reference - AMBICA) / Reference.

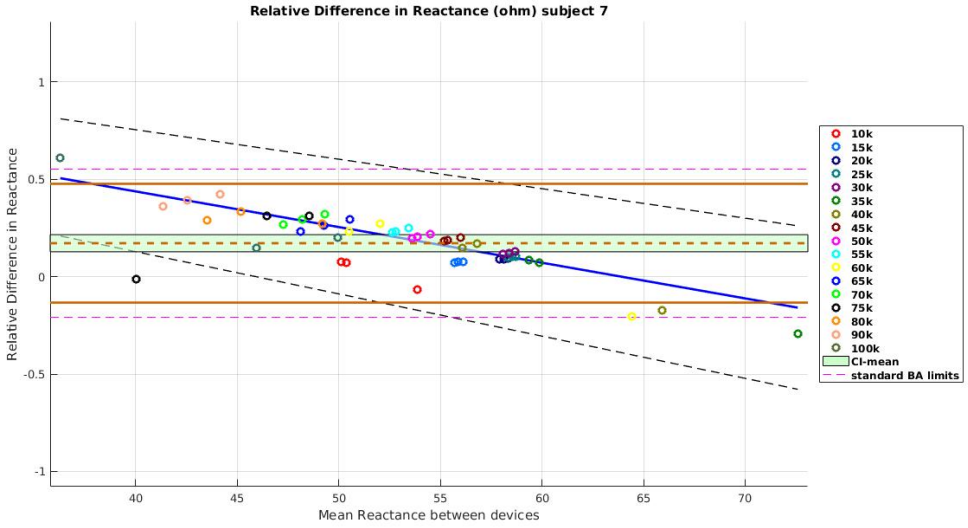

(a) Subject 7 Reactance Plot

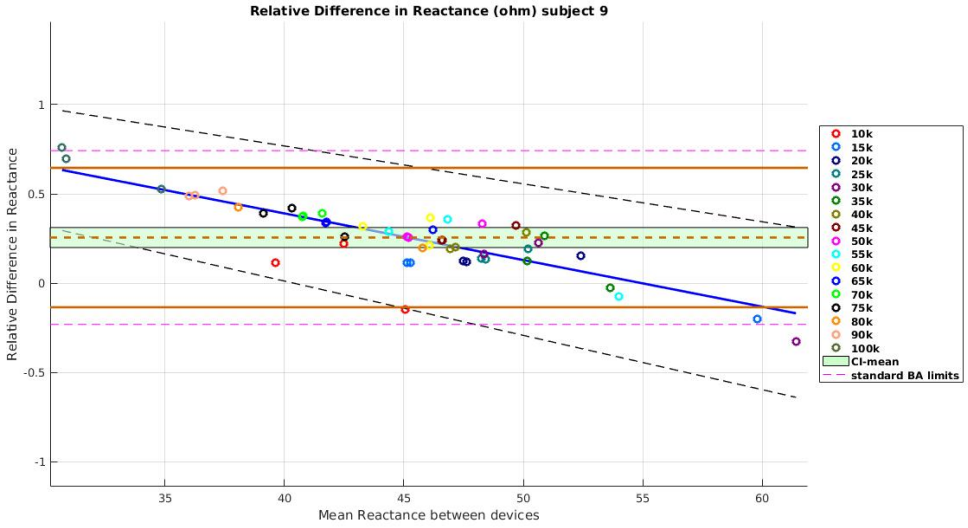

(b) Subject 9 Reactance Plot

Figure A.9: Bland Altman Plots for Reactance Measurements - 3
Note: y-axis is relative difference (Reference - AMBICA) / Reference.

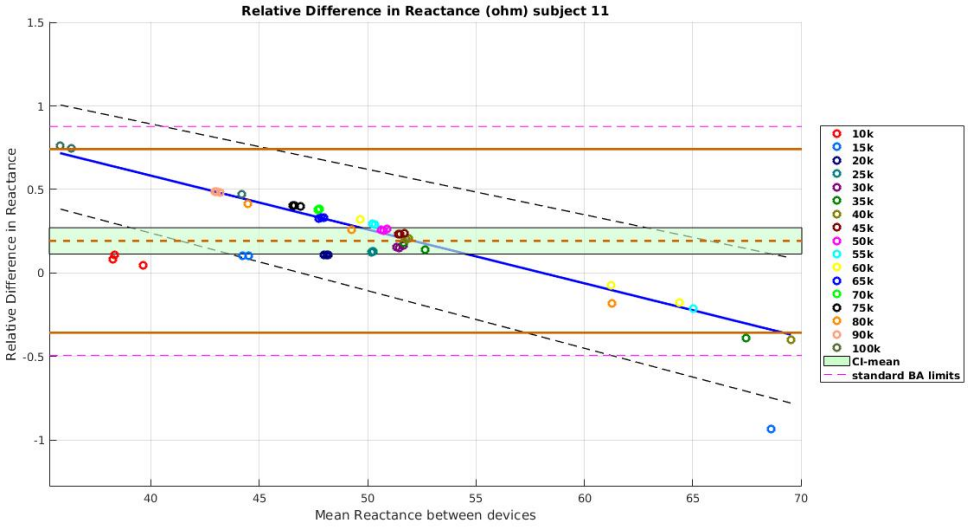

(a) Subject 11 Reactance Plot

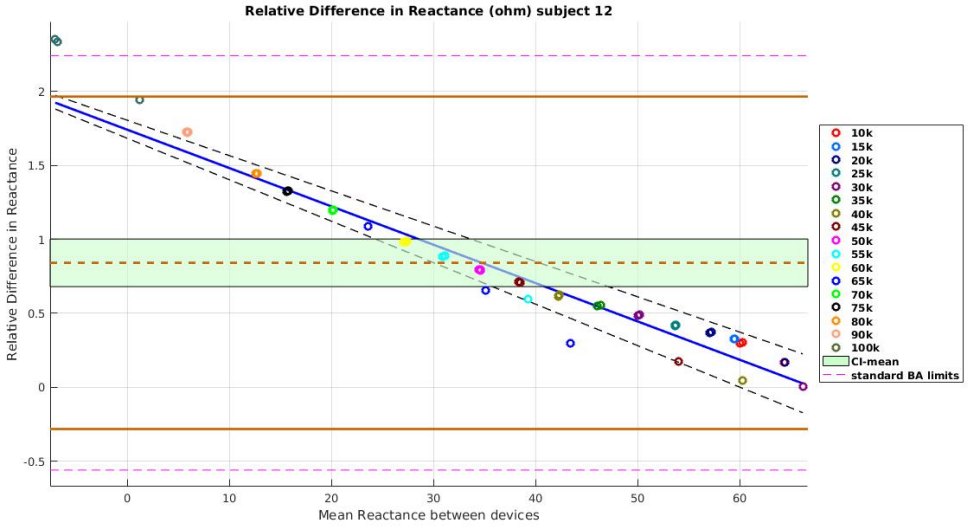

(b) Subject 12 Reactance Plot

Figure A.10: Bland Altman Plots for Reactance Measurements - 4
Note: y-axis is relative difference (Reference - AMBICA) / Reference.

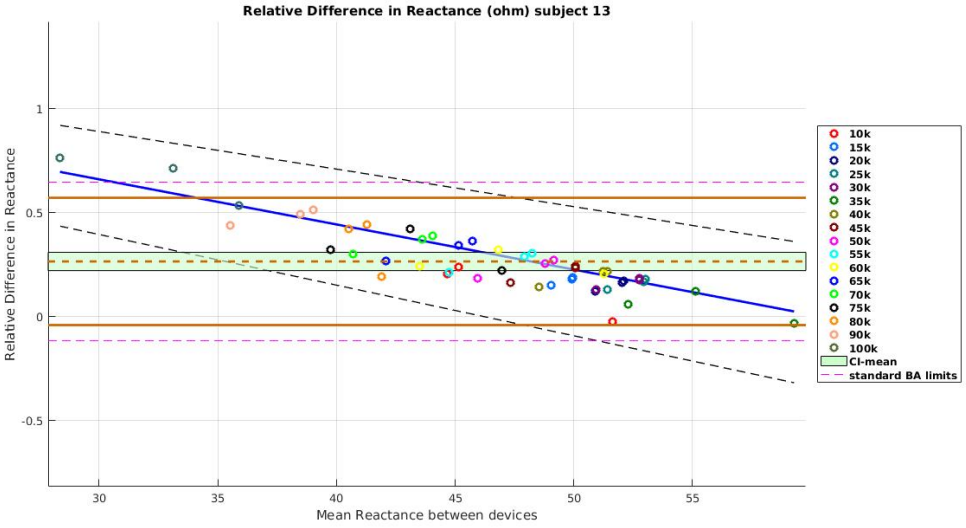

(a) Subject 13 Reactance Plot

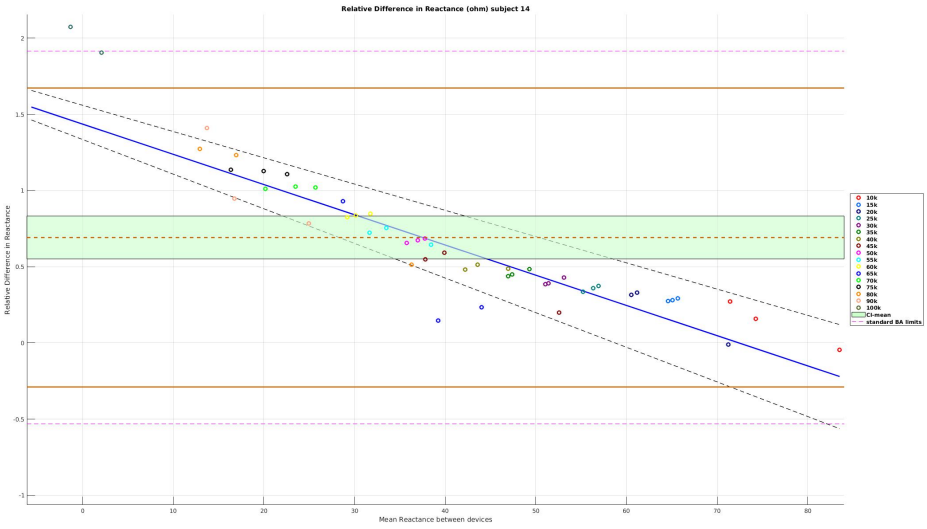

(b) Subject 14 Reactance Plot

Figure A.11: Bland Altman Plots for Reactance Measurements - 5
Note: y-axis is relative difference (Reference - AMBICA) / Reference.

A.3.1 Variation of Difference with Frequency

The trend between difference between measurements and the mean was presented in the Chapter 4.The variation observed was due to the contrasting differences observed at each frequency.Tables A.1 & A.2 below indicate the contrasting behavior.

The average difference between impedance measurements increases from 10kHz to 55-60kHz and beyond it it begins to decrease.The least average difference measured is at 10kHz.From the standard deviations of the difference,it is observed that the variability is quite high.This is particularly due to the large individual impedance discrepancy contributed by subjects 1 and 14.

Table A.2 shows a very definitive trend where as the frequency increases the measured average difference increased.The least average difference was observed at 25kHz and the ,maximum difference at 100KHz.

Frequency	10kHz	15kHz	20kHz	25kHz	30kHz	35kHz	40kHz	45kHz
Average Difference	-1.35	-2.06	-3.04	-2.76	-3.01	-3.61	-3.78	-3.86
SD	9.41	8.72	9.68	9.30	9.65	10.22	10.74	11.12
Frequency	50kHz	55kHz	60kHz	65kHz	70kHz	80kHz	90kHz	100kHz
Average Difference	-4.06	-3.77	-3.15	-3.02	-2.45	-2.93	-3.19	-2.47
SD	11.61	11.54	14.18	11.42	14.03	13.03	14.22	12.65

Table A.1: Frequency wise difference in impedance measurements between AMBICA and reference device observed for all subjects. SD : standard deviation of differences.

Frequency	10kHz	15kHz	20kHz	25kHz	30kHz	35kHz	40kHz	45kHz
Average Difference	4.61	3.719	0.64	6.78	6.55	7.21	5.53	10.146
SD	7.13	11.46	11.49	9.32	11.33	12.75	14.42	13.25
Frequency	50kHz	55kHz	60kHz	65kHz	70kHz	80kHz	90kHz	100kHz
Average Difference	10.99	12.36	13.34	11.26	12.97	16.75	18.67	28.28
SD	15.33	15.77	18.97	16.55	20.04	21.05	23.70	28.36

Table A.2: Frequency wise difference in reactance measurements between AMBICA and reference device observed for all subjects. SD : standard deviation of differences.

A.3.2 Box Plots - Features Extracted

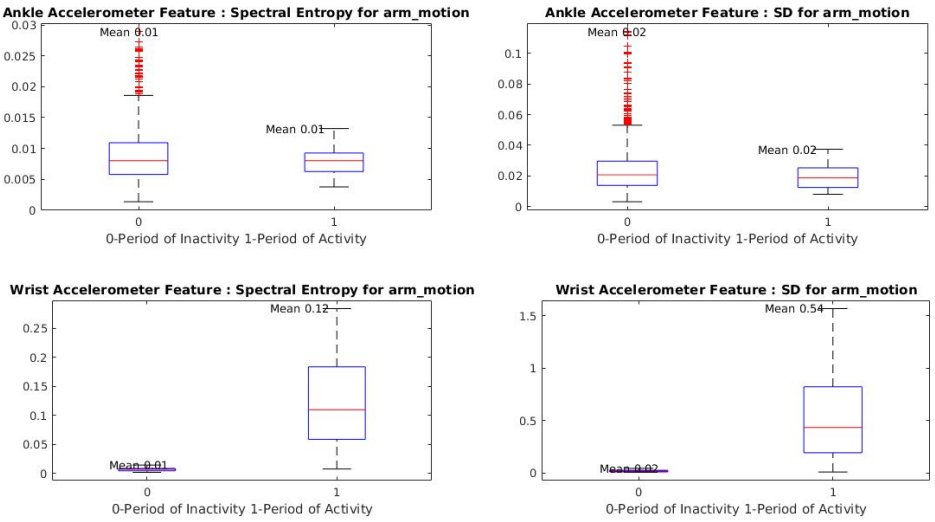

(a) Magnitude of features extracted during Arm Motion

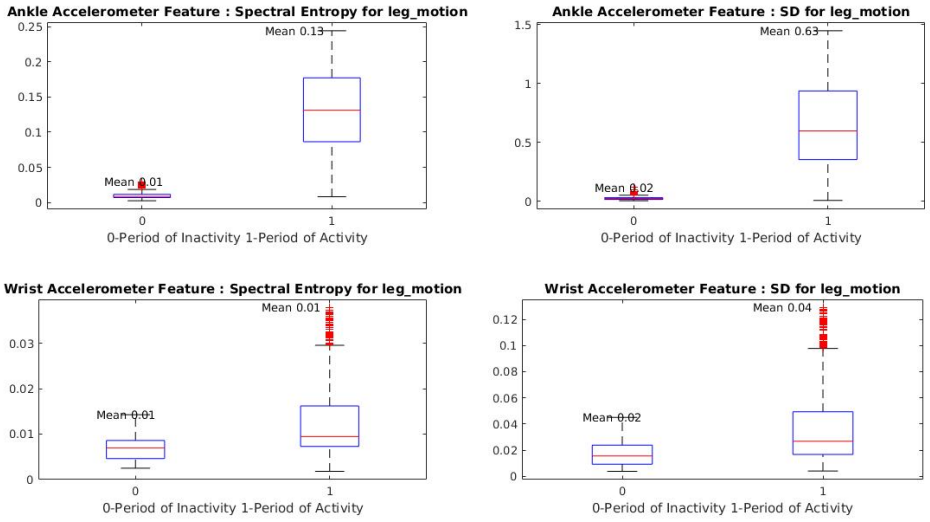

(b) Magnitude of features extracted during Leg Motion

Figure A.12: Box plots showing the magnitude of feature extracted for wrist and ankle rotation

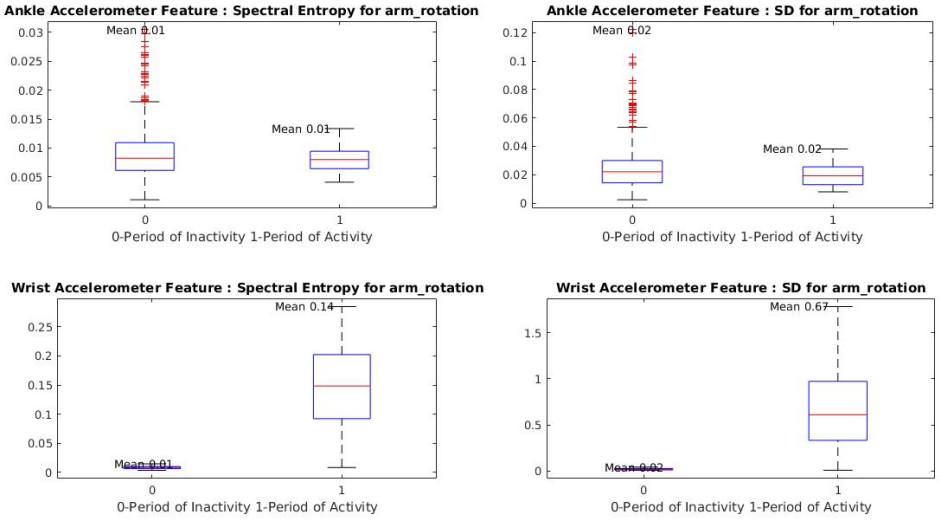

(a) Magnitude of features extracted during Arm Rotation

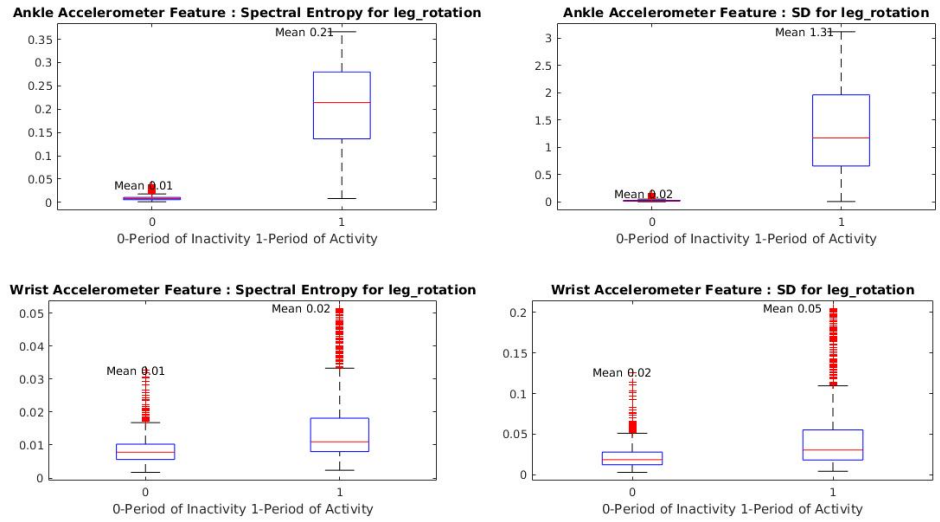

(b) Magnitude of features extracted during Leg Rotation

Figure A.13: Box plots showing the magnitude of feature extracted for wrist and ankle rotation

A.3.3 Average Loss per fold for each models

Folds	Loss for Decision Tree	Loss for SVM
1	0.022	0.030
2	0.025	0.028
3	0.019	0.021
4	0.025	0.028
5	0.031	0.033
6	0.028	0.033
7	0.019	0.021
8	0.025	0.030
9	0.024	0.026
10	0.019	0.020

Table A.3: Average loss per fold for each model